People's Democratic Republic of Algeria
Ministry of Higher Education and Scientific Research
University M'Hamed BOUGARA – Boumerdes

Institute of Electrical and Electronic Engineering
Department of Power and Control

Final Year Project Report Presented in Partial Fulfilment of the Requirementsfor the Degree of

MASTER

In **Power Engineering**

Option: **Power Engineering**

Title:

Power Flow Analysis for AC Islanded Microgrids

Presented by:

- **BELAYATI Abderraouf**
- **BOUDALI Mouhammed Amine**

Supervisor:

Pr. A. KHELDOUN

Registration Number:………/2021

Dedication

“To my Mother, to my lovely sister and her husband. I am deeply grateful to all of you for your support and unconditional love during all my studies. You gave me a dream, and I am proud to hold a part of its reality. To all my friends and classmates, especially Radhouane Hammachi, Malik Kissoum and Nadhir boukorsi. Thank you all for the enjoyable time I spent with you, your encouragement and support, and the unique experience I had with you.”

∞ *Amine* ∞

“I dedicate all people who are a part from my career and this project; I salute each one of them for all kind of the provided encouragements and the supports”

∞ *Abderraouf* ∞

Abstract

The cluster of micro sources, storage devices integrated to power electronic interface to meet the load demand forms a small distributed network termed as a microgrid. The capability of the microgrid to act autonomously is an islanded microgrid, which fulfils the object of electrifying the remote areas by means of renewable sources. In an islanded Microgrid (MG), the use of conventional power flow analysis is not effective as the voltage of slack bus and the frequency of the MG are assumed to be constant. Such assumption fails to consider the real characteristics of the islanded MG as all distributed generators (DGs) are involved in providing the demand of active and reactive power as well as maintaining the frequency of the MG.

In this project, simple algorithms are proposed for load flow solutions in islanded MGs to evaluate the frequency, Distributed generators active and reactive powers, voltage magnitudes and angles using Newton Raphson method with droop control-based concepts. The proposed methods are applied to 6-bus, 7-bus and 18-bus test systems and simulated based on the combination of two well-known software products, namely MATLAB and OpenDSS. The results are compared with time domain simulations conducted by PSIM which validate the effectiveness of the developed algorithms. In all cases, trivial differences are observed, validating the accuracy and the robustness of the proposed approaches.

Acknowledgment

First of all, we would like to express our endless thanks to our supervisor, who accepted to supervise us for the realization of this work **Prof. Aissa KHELDOUN** for his kindness, encouragements, enthusiastic guidance, helpful advice and technical supports throughout our research. Without his motivation and instructions, the thesis would have been impossible to be done effectively. We are so grateful for all of the assistance he has provided throughout the year, his cooperation and his valuable suggestions. He was so helpful in lending his expertise and knowledge and ensuring that our work is progressing in perfect way. It was so comfortable and enjoyable to work with him.

We would like to thank our professors, our collages, and all our friends. Our appreciation is also extended to all institute teachers for their helps during the whole academic years.

Finally, we thank so much all persons who contributed in the completion of this work, as well as, our friends and our families who support and encourage us over the whole project.

Table of Contents

List of Tables

List of Figures

List of Abbreviations

AC	**A**lternative **C**urrent
CPF	**C**onventional **P**ower **F**low
CHP	**C**ombined **H**eat and **P**ower
CP	**C**onstant **P**ower
CZ	**C**onstant **I**mpendence
DER	**D**istributed **E**nergy **R**esources
DG	**D**istributed **G**enerators
DMS	**D**istribution **M**anagement **S**ystem
DSS	**D**istribution **S**ystem **S**imulator
FDLF	**F**ast-**D**ecoupled **L**oad **F**low
FES	**F**lywheel **E**nergy **S**torage
HAWT	**H**orizontal **A**xis **W**ind **T**urbines
LMI	**L**inear **M**atrix **I**nequality
LC	**L**oad **C**ontrollers
LV	**L**ow **V**oltage
MPPT	**M**aximum **P**ower **P**oint **T**racking
MGCC	**M**icrogrid **S**ystem **C**entral **C**ontroller
MC	**M**icro **S**ource **C**ontrollers
NR	**N**ewton **R**aphson
PFA	**P**ower **F**low **A**nalysis
PFS	**P**ower **F**low **S**ystem
PS	**P**ower **S**ystem

PV	**P**hoto-**V**oltaic
RES	**R**enewable **E**nergy **S**ource
PV	**S**olar **P**hotovoltaic
THD	**T**otal **H**armonic **D**istortion
VAWT	**V**ertical **A**xis **W**ind **T**urbine

General Introduction

The intermittent and random production of renewable sources, such as photovoltaic and wind turbine, is always a problem for their large-scale integration in the utility grid. One of the solutions is to group renewable sources, traditional sources, storage and local consumption and treat it as a single unit in the utility grid. This is the concept of microgrid. Such concept emerged as one of the most promising technologies to modernize current power system, being able to operate in both grid-connected and islanded mode. A microgrid has the potentials of better responding both grid and end-user requirement, it facilitate the implementation of future smart grid. [1]

The electric power system is a complex system that requires a thorough design and operation process. The first step in designing a (future expansion of) power system is a power flow study. A power flow study is a numerical analysis to determine the flow of electric power in a system by calculating the voltage magnitude and angle of every bus in the network. As electricity demand continues to grow and the technology around renewable energy sources (RES) matures, we see more and more RES being integrated into the electric power system. However, the distributed nature and intermittency of the RES, as well as the power-electronic interfaces of most loads and RES bring challenges, and require modifications in the existing power system operation practices, including the power flow studies. [2]

The power flow problem can be easily tackled in grid connected MGs by applying conventional power flow (CPF) methods, such as the Newton Raphson and the Gauss-Seidel, these methods are based on the concept of the slack bus, which is used to simulate the utility grid, in this concept the grid frequency is predetermined, and voltage magnitude of the slack bus is assumed constant and a priori known , whereas in islanded mode the consideration of the slack bus, operating at fixed voltage and frequency is not valid thus, the use of conventional power flow analysis in islanded mode is not effective hence , new concepts and algorithms are developed to solve the load flow problem.[3]

This research aims to provide novel and accurate steady-state power flow analysis methods that address the unique characteristics of networked islanded microgrids and can be easily implemented and expanded to various topologies considered the droop characteristics of the distributed generators (DGs) Using the conventional power flow system PFS, Newton-Raphson is performed with a random selected slack bus. The main advantage of these methods is to calculate the DGs active and reactive powers that satisfy the load demand with minimum losses and avoid frequency and voltage oscillations to operate in stable and efficient mode.

The thesis is organized in four chapters:

Chapter 1 provides a literature review of the definitions and concepts of microgrids as well as the different types of MGs, type of DGs and energy storage.

Chapter 2 covers conventional load flow solutions which can be applied to the conventional grid or grid connected microgrid.

Chapter 3 describes the non-conventional methods for performing the power flow of the islanded microgrid

Chapter 4 in this chapter a simulation is performed for the islanded microgrid using non-conventional with different algorithms and networks and a comparison between them is deduced.

Chapter 1

Introduction to Microgrid Concept

1.1. Introduction

The rapid move toward using distributed renewable energy resources as a replacement for large fossil fuel power stations is enforcing a major re-think on the existing distribution and transmission models used by the energy industry.

One increasingly popular solution is to connect up distributed resources in local microgrid whether in urban areas, which are rapidly adopting rooftop solar, or in remote locations, where solar and wind can power off-grid networks. [4]

1.2. Brief History of Microgrid

The microgrid concept dates back to the beginning of our industry. In 1882 when Thomas Edison opened his Pearl Street Station there was no standard for a generation-distribution system for electricity, so he designed as he went along. Amazingly, Edison's Manhattan Pearl Street Station met all of today's criteria for what is today's microgrid system. It was self-contained and powered by coal fired steam engines that drove six jumbo generators. Each of his generators produces 1,100 kW direct current (DC).

As with most microgrids, Edison's electric system was small with localized generation and a limited distribution network. It only served a few blocks in any direction because of the restrictions of the DC transmission network, which fits today's definition of a microgrid. Interestingly, it also included batteries to provide energy storage. Microgrids with energy storage are a very hot topic today, so once again Edison was thinking ahead. His system also supplied heat from its steam generation to buildings around its facilities. Today we call this combined heat and power (CHP). Once again Edison's ideas were spot on. CHP has proven to be very valuable.

Even though modern microgrids have been part of the grid for many years most of us had not heard of a microgrid until Superstorm Sandy hit the United States in 2012. The northeastern part of the U.S. including New York City lost electrical power for many weeks, but many customers noticed not everyone lost power. Lights were on in some buildings in New York, New Jersey and Connecticut because they had microgrids or distributed generation. This got a lot of attention from the politicians in charge because of their constituents. As a result, microgrids were included in the rebuild of the power grid in this area and as they say, the rest is history. [5]

1.3. Conventional electrical networks

Conventional electrical supply network usually consists of generation, transmission, distribution, and consumer (load) systems. Generation system normally consists of a combination of large-scale centralized generation plants. A typical modern generating unit has rated value of over 1,000 MW. A transmission system is specifically designed to transfer bulk of power from generating plants to distribution systems at high- and extra-high voltage levels over long distances. Typical operating voltages of transmission systems include 400 kV, 220 kV and 60 kV. Distribution systems, however, are specifically designed to receive electric power from transmission system to be distributed to load centers. It is therefore important to note that the role of a distribution network is passive, that is, its role is confined to transferring electricity from generation and transmission systems to load centers. The operating voltage of distribution networks includes 30kV and 10 kV.

Conventional electrical supply networks normally have vertical structure whereby the electric power generated by the generation system is passed to transmission system which is then transferred to distribution network for feeding it to connected loads.

A conventional vertical power system is being seen as in need of modification to meet the strong requirements of uninterruptible power, growing consumption of electricity in rural and urban areas, mitigating voltage fluctuation problems for far-end loads and overall cost reduction of erecting huge long power transmission networks for feeding remote areas. The concept of one-way power transmission is slowly being replaced in renewable energy sources connected to power system. [6]

It has been recognized that the changes to which electrical networks are subjected in recent years have made the grid of today unable to meet the challenges of the future, this has led to urgent need to modernizing electrical networks, which in turn has evolved into the development of the microgrid Grid concept. The microgrid concept is widely perceived as way forward to solve problems related to growing energy consumption, integration of distributed generation, energy efficiency, power supply reliability, and power quality.

The factors that led to the development of the microgrid concept may be summarized as follows:

● Aging of conventional electrical networks coupled with the emergence of new applications

● Political and environmental factors

● Liberalization of electricity market

● Motivation and inclusion of customers as players to support the grid

1.4. Definitions of Microgrid

There are some definitions of a microgrid in the world. Following the U.S. Department of Energy, MGs are a group of interconnected loads and distributed energy resources within clearly defined electrical boundaries that acts as a single controllable entity with respect to the grid and that connects and disconnects from such grid to enable it to operate in both grid-connected or island mode.

Accordingly, the CIGRE C6.22, microgrids are electricity distribution systems containing loads and distributed energy resources, (such as distributed generators, storage devices, or controllable loads) that can be operated in a controlled, coordinated way either while connected to the main power network or while islanded.

From the CORDIS Europe point of view, a microgrid is defined as a series of electrical loads, elements of generated power supply and storage elements that, connected to the electric grid by means of a single point of connection, are all linked through a strategy that manages both the flow of energy within the grid as well as the interchange of power with the main supply grid.

Basically, a MG is a small-scale power grid that can operate either grid connected mode or autonomous (islanded mode). In the grid-connected mode, it has exchangeability energy between MG and utility. Besides, in the islanded mode, it has self-controlled and self-managed. MG includes distributed generations, storage, control devices and loads. [7]

The **Figure 1.1** shows the topology of microgrid system and its components

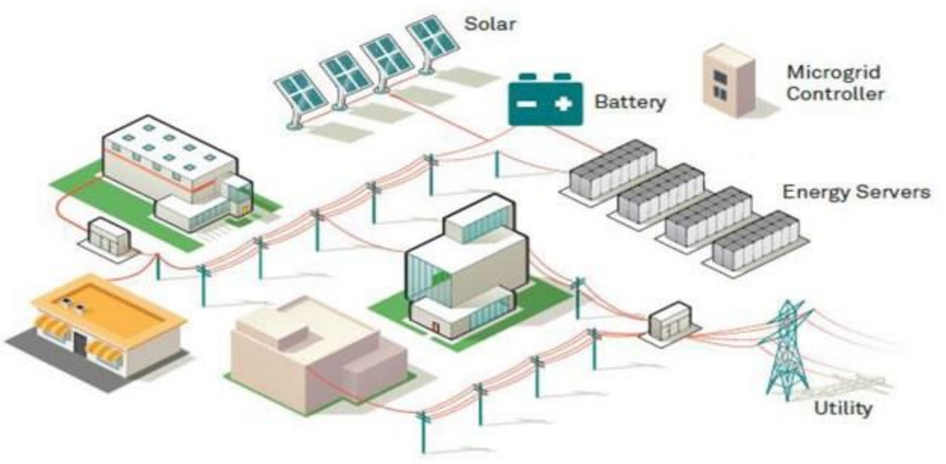

Figure 1.1 Microgrid system topology

1.5. Characteristics of Microgrid

Microgrid is characterized with some valuable aspect which can be resumed as follow:

Independence: MG can operate in islanded mode. In autonomous operation, MG is capable of balancing generation and load. Besides, it can keep system voltage and frequency in defined limits with adequate controls.

Flexibility: The expansion and growth rate of MGs do not need to follow any precise forecasts. According to operation modes, MGs can operate in different modes. Connecting to the main grid is optional.

Stability: MG can operate stably during nominal operating modes and transient events, no matter whether the larger grid is up or down (Additional research is required).

Interactivity: MGs are compatible with the main grid. They can support the main grid if it is necessary and the main grid can also supply for MGs.

Expanse: MGs can grow easily by adding more distributed energy resources (DERs) and loads. It is easier than expand the traditional grid.

Efficiency: The utilization of DERs optimization and manage loads by using centralized as well as distributed MG controller is the way to make energy management goals optimization. [8]

1.6. Microgrid Structure

➢ Alternative Current (AC) Microgrid

The structure of AC microgrid shows in **Figure 1.2**. In an AC microgrid, DERs are connected to an AC bus through power electronic devices and supply power for the loads.

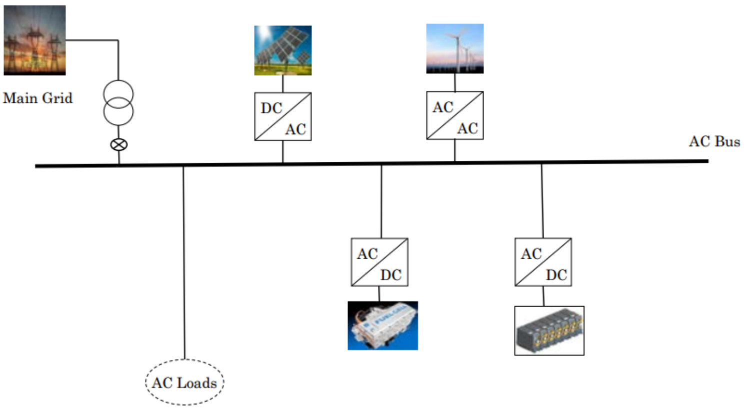

Figure 1.2 Typical structure of a AC microgrid.

This architecture is characterized with the advantages of easily modifying the voltage levels through the utilization of transformers and of having high fault management capability i.e., detecting and handling the faults with the wide range of protection devices. However, it presents some draw backs such as the need of synchronization of distributed generation or the circulation of reactive power that increases the power losses in the transmission system.

➢ DC Microgrid

In DC microgrid, DERs and loads are connected to DC bus through power electronic devices. Besides, DC microgrid is connected to the main grid through an inverter, as shown in **Figure 1.3** DC microgrid includes DC power sources and loads are more economical.

In fact, since various distributed generation sources e.g., solar photo voltaic (PV), fuel cells, batteries, etc. and also various loads e.g., lighting, heating, ventilation, etc. output or accept DC power, these microgrids have been proposed to avoid losses from converting power between DC and AC.

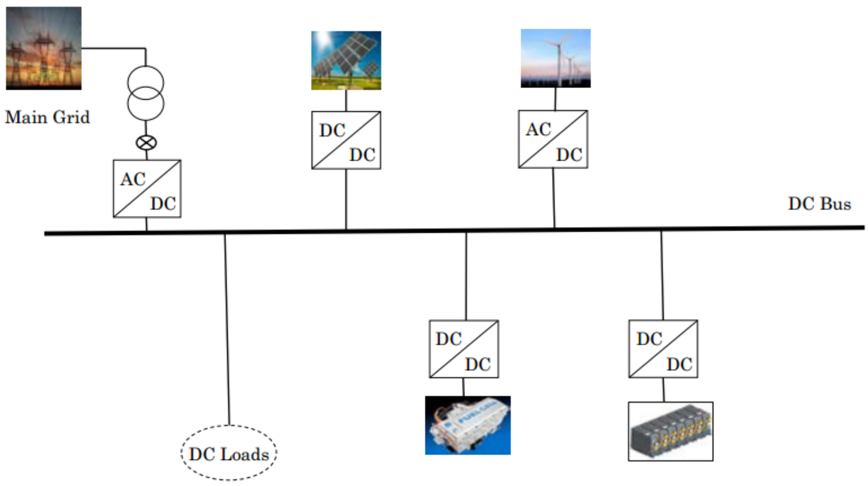

Figure 1.3 Typical structure of a DC microgrid.

Note that losses on traditional AC-type systems including the conversion stages (from AC to DC) and cables (losses associated with skin effects and reactive power flow) typically range from 5% to 15% of power generation. Given the reduction in losses, DC microgrids come with a decreased requirement for cooling and ventilation systems due to the fact that less energy is dissipated as heat through the conversion stages, which can be considered a critical factor in applications with intense power usage and several DC-type sources, such as data centers, commercial electric vehicle charging stations, etc. Adding to these the fact that faults in DC systems can be isolated with blocking diodes, and issues of synchronization, circulating reactive currents, and harmonic distortion are alleviated, then it becomes clear why they are considered to be a valuable resource.

Even, though, significant research has been dedicated recently in DC microgrids due to the profound benefits briefly mentioned above, there are some issues that hinder their large-scale deployment. The major of these is the lack of standardization, i.e., no standard voltages exist that dictate the use of a nominal voltage for a certain application. For example, we know that AC homes typically operate at a low voltage equal to 230 V, but such a nominal profile for DC homes has not been widely adopted by the industry. Standardization efforts have increased in recent years, such as the research outputs produced by Fraunhofer Research Institute that suggest two voltage levels for DC buildings, these being 380 V DC (for higher load application, i.e., whole buildings) and 24 or 48 V DC (for lower load application, i.e., single homes). These standardization efforts have been summarized in the Emerge Alliance Data/Telecom Center and Occupied Space Standards and more importantly in the IEC 60038 Standard which defines a set of standard voltages for use in low voltage (including DC systems). Apart from the major issue of standardization, for large-scale deployment of DC systems significant modification of the current distribution networks would be required, hence they would only be considered an attractive option for small-scale, remote or isolated systems.

- **Hybrid AC/DC Microgrid**

A third option, which has attracted a lot of attention lately, is the hybrid AC/DC microgrids. This configuration combines the advantages of AC and DC architectures as the two sub-networks are connected with the same distribution grid enhancing the integration of both AC and DC based distributed generation resources, energy storage devices and loads. As such, they pose an efficient way for the increased penetration of renewable energy technologies, batteries and even electric vehicles without the need for great modifications, hence with a reduced capital cost. A typical AC/DC microgrid is depicted in **Figure 1.4.**

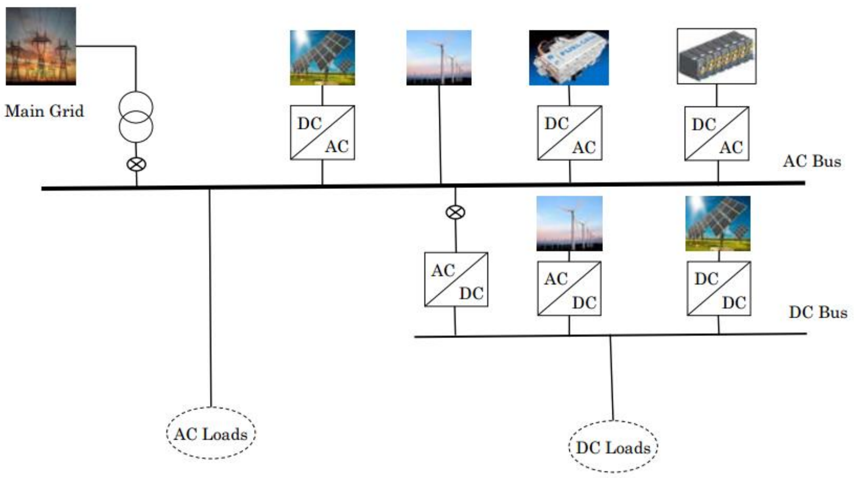

Figure 1.4 Typical structure of a Hybrid AC/DC microgrid.

As it can be observed in **Figure 1.4**, in a hybrid AC/DC microgrid, AC-type units such as wind turbines and AC loads are connected to an AC bus, while DC-type units such as solar PV, electric vehicles, energy storage devices and DC loads are connected to DC bus bar. The two sub grids are interconnected through the so-called interlinking converter; this can be one or multiple depending on their ratings and those of the sub grids. It is a bidirectional converter which, through its special controllability, performs multiple functions essential for the optimal operation of hybrid AC/DC microgrids. As an example, power sharing through the two sub grids is enabled via a droop control strategy implemented in the interlinking converter.

A non-exhaustive list of advantages of the hybrid AC/DC microgrids is provided hereafter:

- Reduction of conversion stages: It leads to reduced capital required in the planning stage of the microgrid and reduced losses in the operational stages.
- Improved reliability: The decoupling of the AC and DC sub grids can prove to be a beneficial factor under abnormal conditions. When a disturbance occurs in the AC sub-grid that will disrupt power generation on this side, the DC one will transfer any surplus power to cover the demand and reduce load curtailment.
- Harmonics reduction: Reduction of the conversion stages results in increased power quality that would otherwise be impacted by the harmonics generated from the various converters.
- Environmentally friendly: Hybrid AC/DC microgrids can enhance the maximization of renewable energy sources, especially since no additional capital is required for converters, which in turn leads to minimization of green energy wasted.
- Unbalanced loads: Negative and zero sequence current problems caused by unbalanced loads in the AC subgride can be mitigated by the DC sub-grid. [8]

1.7. Physical Components of Microgrid

Every micro-grid design must use the best technology available to meet its specific objectives. The micro-grid technology framework consists of micro-resources like PV arrays, wind generators, fuel cells, micro-turbines, biomass, geothermal, steam or gas turbines. The storage devices in MGs can include flywheels, energy capacitors (super capacitors), and batteries.

I. Distributed Generation

DERs are generally modular units of small capacity due to their lower energy density and their dependency on geographical conditions of a region. They are usually located close to the loads and are also geographically widespread. Generating power at low voltage (LV) level makes it possible to connect DERs individually to the distribution network or work interconnected in the form of microgrids. As a separate semi-autonomous entity, the microgrid can again be reconnected to the network.

- *Solar PV*: Solar PV is a technology that converts sunlight into direct current electricity by using semi-conductors [9]. Typically, PV cells are pre-wired in series to form a PV module. Multiple modules, in turn can be wired together to form an array, which can be scaled up or down to produce the amount of power needed. PV cells can be made from various semi-conductor materials but the most commonly used material today is silicon.
- *Wind turbine:* A wind turbine is a type of electric power generator which converts the kinetic energy of the wind into electrical energy. The wind energy is a result of the difference in atmospheric pressure from one region to another; this energy depends on
  - The amount of air (Volume)
  - The speed of air (Velocity)
  - The mass of air (Density)

Wind turbines fall into one of two categories: Horizontal axis wind turbines (HAWTs) and vertical axis wind turbines (VAWTs). HAWTs are the more common type.

- *Full Cell:* A pollution free electrical generation technology that convert the chemical energy of a fuel directly into electricity. The source fuel could be almost anything that can be oxidized, including hydrogen, methane, propane, methanol, diesel fuel or gasoline. In many respects, a fuel cell resembles a battery, but over a much longer period of time it can supply electrical energy. For this reason, they have been used for decades in space probes, satellites, and manned spacecraft. Nowadays, fuel cells are mostly used in utility power plants, hospital and cars.

II. Energy Storage Systems

Modern storage systems are unique in that they are very fast responding resources that can both generate and absorb power and, in some cases, regulate real and reactive power quality in an electric distribution system. These capabilities allow storage to serve a variety of roles within a microgrid for instances where customers have a need for uninterrupted islanding, have no on-site generation, or need to supplement the on-site generation that exists in their distribution system.[10]

- Flywheel Energy Storage Systems (FES)

Flywheel refers to a rotating mass that stores energy in the form of kinetic energy. It can serve as a short-term backup power source when the main energy source fails. The FES has been deployed in many applications, which include—but are not limited to—space systems, telecommunications, and data centers. [11]

- Energy Storage Super-capacitor

The super capacitor is an electrochemical device, so the energy storage processes are reversible with no chemical reactions. Therefore, the super-capacitor can be repeated charge and discharge hundreds of thousands of times. Its power density is 10-100 times more than that of conventional batteries, so it applies to short-term high power output; it could complete the process of charging tens of seconds to minutes due to its fast charging ability, without testing whether it is full, and its over-charge is risk free; it has long life and low-temperature performance. Hence, using super-capacitor as the energy storage device is ideal for applications in a variety of systems.

- Batteries

Batteries are electrochemical energy storage devices. There are different forms of batteries: lithium-ion, lead acid, sodium, and others designed to meet specific power and duration requirements. They allow storing the excess of renewable energy for later use to ensure continuity of supply. The main disadvantage for a battery is short lifespan.

1.8. Control of Microgrid

In order to achieve a desired flexibility, the MG system in controlled and managed by programmable logic controllers.

The MG controllers are composed mainly from:

- Micro Source Controllers (MC) and Load Controllers (LC)
- Microgrid System Central Controller (MGCC)
- Distribution Management System (DMS).

Depending upon the mode under which a microgrid operates, control strategies are designed. The **Figure 1.5** shows the structure of automation and control of MG.

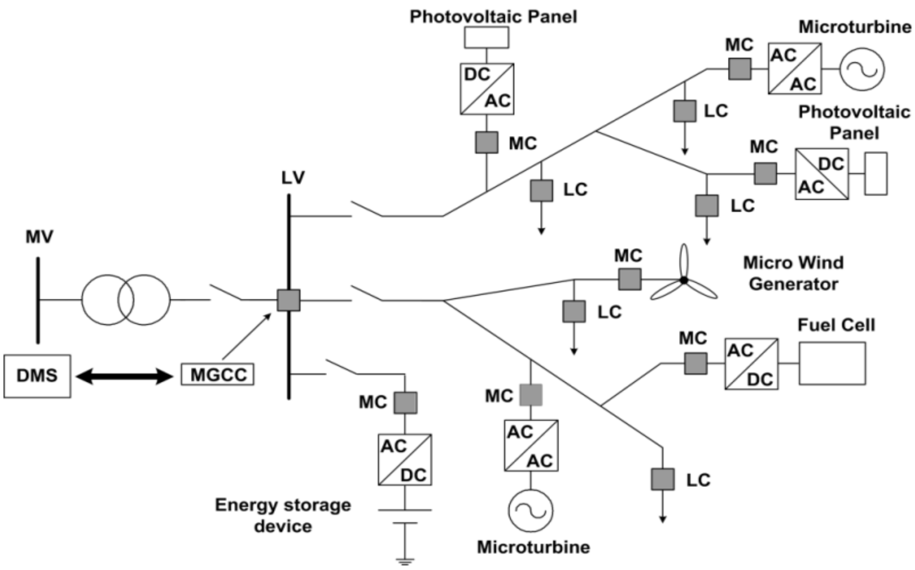

Figure 1.5 Microgrid Automation and Control

1) Grid connected mode

In grid connected mode/on-grid, DG is connected to the utility grid at the Point of Common Coupling through STS (Static Transfer Switch). The amount of active and reactive power to be injected by a DG is decided by the MGCC. MGCC issues commands to the MCs and LCs and these devices in turn control the local devices. Communication between MGCC, MCs and LCs is to transfer the small information related to set points of active and reactive power, reference voltage and frequency etc., PQ control is employed in this mode to regulate active and reactive power from inverter.

2) Islanded mode

When the microgrid is working autonomously, it enters into this mode due to maintenance, outage or economic reasons. Inverters acting as Voltage Source Inverters in this mode require voltage and frequency set points which can be obtained by centralized or decentralized control.[12]

1.9. Advantages and Disadvantages of MGs

The development of microgrid is very promising for the electric energy industry because of the following advantages:

➢ Advantages of Microgrids

- Energy efficiency.
- Minimization of overall energy consumption.
- More environmentally friendly.
- More flexible.
- Improvement of energy system reliability.
- MGs can be integrated into existing systems without having to interrupt the load.

In spite of potential benefits, development of microgrid suffers from several challenges and potential drawbacks

➢ Disadvantages of Microgrids

- Voltage, frequency, and power quality should be at acceptable limits.
- Requires battery tanks to store which requires space and maintenance.
- Resynchronization to the utility grid is difficult and complex protection.
- The absence of reactive power in DC MG which is required by most AC loads

1.10. Conclusion

This chapter presents fundamental introduction of microgrid concept with its components and different operation modes. Moreover, active distribution networks and required control and source infrastructures have been introduced. The most widely used renewable energy sources such as wind turbines and solar PV plants have been presented in brief following the active distribution networks.

The micro-grid can be considered as a controlled cell of the power system for the utility purpose whereas, to the consumer the micro-grid can be planned to meet their special requirements such as, enhancement of local reliability, reduction of feeder loses, and local voltages support. Microgrids are a compact version of traditional power system connection multiple distributed sources to multiple loads, which draws the interest of power system planners as they can be of great importance when it comes to electrifying remote areas.

Chapter 2

Power Flow Analysis for Conventional Grid

2.1. Introduction

Load flow analysis is the most important and essential approach to investigating problems in power system operating and planning. Based on a specified generating state and transmission network structure, load flow analysis solves the steady operation state with node voltages and branch power flow in the power system. Load flow analysis can provide a balanced steady operation state of the power system, without considering system transient processes. Hence, the mathematic model of load flow problem is a nonlinear algebraic equation system without differential equations. [13]

The power system includes a bus, which is the vertical line linking several components like the load, generator, feeder, and others. These buses are related to the quantities often measured when referring to an electrical system.

2.2. Classification of Bas Bars

Buses in the load flow analysis are placed in three categories depending on the specified quantities: generation bus, the load bus, and slack bus.

Generation Bus

The generation bus, also known as the PV bus, voltage-controlled bus, or generator bus, represents the generator stations found in a power system. The quantities specified for this type of bus are voltage magnitude and the real power. It means that the unknown variables for the generation bus are the phase angle of voltage and reactive power.

Generators in the power system are connected to this type of bus. Therefore, the bus voltage corresponds to the generator’s voltage, and the generation of active power is correlated to the generator rating specific to the bus.

The voltage magnitude of the generator bus is kept steady by adjusting the synchronous generator’s field current. Real power generation for every generator is assigned concerning economic dispatch.

Load Bus

The load bus, or PQ bus as it is often called, is a type of node that has both the reactive and active power incorporated into the network. It means that the phase angle and voltage magnitude are unknown and need to be calculated using the load flow equation. No generator is connected to the load bus. Voltage in this type of bus may vary within tolerable values, while the phase angle of the voltage is not very crucial for the load. The load bus is the most numerous bus type typically found in the power system.

Slack Bus

The slack bus is often referred to as the swing bus or reference bus. It does not carry any load yet assumed to be real so that losses can be considered during the transmission of power. The generator bus delivers active power, but it does not mean that all of it will be consumed by the load bus. It results in a difference or power loss, which can only be calculated following the load flow solution. The slack bus supplies the complex losses and always has an attached generator so that unfulfilled demand from other buses can be met.

The slack bus maintains the balance of power in the system and is where the generation is made available. The phase angle and magnitude are given, with the angle set to a reference point or zero degrees. All the other phase angles of the other buses are expressed using the swing bus voltage phasor as their reference. [14]

Table 2.1 Bus Classification in Power System

Bus type	**Specified quantities**	**Quantities to be obtained**
Generation bus	P, $\lvert V \rvert$	Q, δ
Load bus	P, Q	$\lvert V \rvert$, δ
Slack bus	$\lvert V \rvert$, δ	P, Q

2.3. Node Power Equations

The problem that we face while analyzing power flow for a system, we don’t know neither the complex bus voltages or the complex injected currents, rather we know the complex consumed and the injected power, therefore we cannot use the directly Y_{bus} equations.

$$\boldsymbol{V_{node}} = \boldsymbol{Y_{bus}^{-1}} \cdot \boldsymbol{I_{inj}} \tag{2.1}$$

Where:

Y_{bus}: the admittance bus matrix, $Y_{bus} = \begin{bmatrix} Y11 & \cdots & Y22 \\ \vdots & \ddots & \vdots \\ Yn1 & \cdots & Ynn \end{bmatrix}$

I, V: the current, voltage of the bus in the vector form respectively.

The advantages of the bus admittance matrix.

- The data preparation of the bus admittance matrix is very simple.
- The formation of the bus admittance matrix and their modification is easy.
- The bus admittance matrix is a sparse matrix thus the computer memory requirement is less. [15]

From **(2.1):**

$$\boldsymbol{I}_{inj} = \boldsymbol{Y}_{bus} \cdot \boldsymbol{V}_{node} \tag{1.2}$$

For any current I_k:

$$I_k = \sum_{n=1}^{N} Y_{Kn} . V_n \tag{2.3}$$

As a result:

$$S_k{}^* = P_k - jQ_K = V_k{}^* I_k = V_k{}^* . \sum_{n=1}^{N} Y_{Kn} . V_n \text{ , } K = 1 \dots . N \tag{2.4}$$

Knowing that:

$$\begin{cases} V_n = |V_n| . e^{j\delta_n} & (2.5) \\ \quad and & \\ Y_{kn} = |Y_{kn}| . e^{j\theta_{kn}} & (2.6) \end{cases}$$

Substituting **(2.5)** and **(2.6)** in **(2.4)**:

$$P_k - jQ_K = |V_k| . \sum_{n=1}^{N} |Y_{kn}| . |V_n| . e^{j(\delta_n + \theta_{kn} - \delta_K)} \text{ , } K = 1 \dots . N \tag{2.7}$$

This is in phasor form, and resolving into real and imaginary parts:

$$P_k = \boldsymbol{V}_k . \sum_{n=1}^{N} \boldsymbol{Y}_{kn} \boldsymbol{V}_n . \cos(\delta_n + \theta_{kn} - \delta_K) \quad \textbf{(2.8)}$$

$$Q_k = -\boldsymbol{V}_k . \sum_{n=1}^{N} \boldsymbol{Y}_{kn} \boldsymbol{V}_n . \sin(\delta_n + \theta_{kn} - \delta_K) \quad \textbf{(2.9)}$$

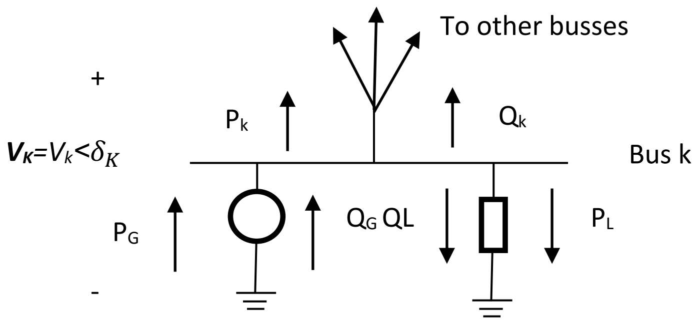

Figure 2.1 Bus variables V_k, δ_K, P_k, and Q_k

The power-flow program. For convenience, the power delivered to bus k in **Figure 2.1** is separated into generator and load terms. That is:

$$\begin{cases} P_k = P_{Gk} - P_{Lk} \\ \quad\quad and \\ Q_k = Q_{Gk} - Q_{Lk} \end{cases} \quad \textbf{(2.10)}$$

We Notice that when bus k is a load bus with no generation, $P_k = -P_{lk}$ isnegative; that is, the real power supplied to bus k in **Figure 2.1** is negative. If the load is inductive,$Q_k = -Q_{lk}$ is negative.

2.4. Power Flow Solutions Techniques

With the advent of the modern digital computers possessing large storage and high speed the mode of power flow studies have changed from analog to digital simulation. A large number of algorithms are developed for digital power flow solutions. The methods basically distinguish between themselves in the rate of convergence, storage requirement and time of computation.

Network equations can be solved in a variety of ways in a systematic manner. The most popular method is node voltage method. When nodal or bus admittances are used complex linear algebraic simultaneous equations will be obtained in terms of nodal or bus currents. However, as in a power system since the nodal currents are not known, but powers are known at almost all the buses, the resulting mathematical equations become non-linear and are required to be solved by interactive methods. Load flow studies are required for power system planning, operation and control as well as for contingency analysis. The bus admittance matrix is invariably utilized in power flow solutions. [16]

The most used numerical techniques to solve the power flow equations are:

- Gauss Seidel method
- Newton Raphson method
- Fast decoupled method

2.4.1. Gauss Seidel Method

i. Basic Concept

To start with, a solution vector is assumed, based on guidance from practical experience in a physical situation. One of the equations is then used to obtain the revised value of a particular variable by substituting in it the present values of the remaining variables. The solution vector is immediately updated in respect of this variable. The process is then repeated for all the variables thereby completing one iteration. The iterative process is then repeated till the solution vector converges within prescribed accuracy. The convergence is quite sensitive to the starting values assumed. Fortunately, in a load flow study a starting vector close to the final solution can be easily identified with previous experience. [17]

From the power balance equation **(2.4)**, we can get:

$$V_k^{(t+1)} = \frac{1}{Y_{kk}}\left[\frac{P_k - jQ_k}{V_k^{*(t)}} - \sum_{\substack{n=1\\ n\neq k}}^{N} Y_{kn}V_n^{(t)}\right] \qquad \textbf{(2.11)}$$

Where:

- P_k , Q_k: are the injected real and reactive power into bus k respectively
- Y_{kk}: Diagonal elements; sum of admittances connected to bus k

- Y_{kn}: Off-diagonals, - (sum of admittances connected between busses k and n)

(2.11) is applied for load busses, and for a generation bus, the reactive power Q_k is calculated firstly with the following equation:

$$Q_K = imag\left[V_k^{(t)}.\left(\sum_{n=1}^{N} Y_{kn}V_n^{(t)}\right)^*\right], K = 1\ldots.N \qquad \textbf{(2.12)}$$

After that, **(2.11)** is used only to calculate the angle of $V_k^{(t+1)}\angle\delta^{(t+1)}$since the voltage magnitude is an input data for the PV bus. [18]

ii. Advantages and disadvantages of Gauss-Seidel Technique

a) Advantages

- Simple and easy technique specially for small systems.
- It needs small computer memory space**.**
- The iteration needs short time to be executed.

b) Disadvantages

- It fails to converge in systems with many bus bars.
- It fails to converge in systems having negative values of transfer admittances and systems with heavily loaded lines, etc.
- The convergence depends on many factors such as: the initial solutions, the acceleration factor, the tolerance limit, the slack bus selection, level of accuracy of results needed. [19]
- Slow rate of convergence resulting a large number of iterations.
- Increasing in the number of iterations with increase in the number of buses.

2.4.2. Newton Raphson Method

i. Basic concept

Gauss-Seidel method was widely used before the introduction of Newton-Raphson method (NR). Currently the Newton-Raphson method is being widely used which is more reliable but has higher memory requirements. The use of sparsity programming and optimal ordering has reduced memory requirements and increased the popularity of the method. [20]

The Newton-Raphson method solves the power flow problem by using a set of non-linear equations to calculate the voltage and phase voltage angle of each bus. The method is applicable for scalar and vector forms, like it is explained in the following:

a) In scalar form

- NR is geared towards solving equations like**:**

$$\mathrm{f}(\hat{x}) = 0 \quad \textbf{(2.13)}$$

- For each $\hat{x}$, we define:

$$\Delta x^{(t)} = \hat{x} - x^{(t)} \quad \textbf{(2.14)}$$

- The expansion of $\mathrm{f}(\hat{x})$ about $\mathrm{f}(x^{(t)})$:

$$\mathrm{f}(\hat{x}) = \mathrm{f}\left(x^{(t)}\right) + \frac{d\mathrm{f}\left(x^{(t)}\right)}{dx}(\Delta\mathrm{f}\left(x^{(t)}\right)) + \frac{1}{2}\frac{d^2\mathrm{f}\left(x^{(t)}\right)}{dx^2}(\Delta\mathrm{f}(x^{(t)}))^2 + \cdots \quad \textbf{(2.15)}$$

- By taking just the first tow terms of **(2.15)**, using this approximation of $\mathrm{f}(\hat{x})$, we solve for $\Delta x^{(t)}$

$$\Delta x^{(t)} = -\left[\frac{df\left(x^{(t)}\right)}{dx}\right]^{-\mathbf{1}} . f\left(x^{(t)}\right) = \hat{x} - x^{(t)} \quad \textbf{(2.16)}$$

- Then, a new estimation is calculated:

$$x^{(t+1)} = x^{(t)} + \Delta x^{(t)} \quad \textbf{(2.17)}$$

- After n iterations, the solution$\hat{x} = x^{(n)}$ is obtained once $\Delta x^{(t)} < \varepsilon$

b) For Vector form

- Now we will extend the Newton method to simultaneous nonlinear equations. Assume the nonlinear equations with N variables:

$$X = \begin{bmatrix} x_1 \\ x_2 \\ \vdots \\ \vdots \\ x_N \end{bmatrix} \quad \textbf{(2.18)}$$

$$F\begin{bmatrix} f_1 \\ f_2 \\ \vdots \\ f_N \end{bmatrix} = \begin{cases} f_1(x_1, x_2, \cdots, x_N) = 0 \\ f_2(x_1, x_2, \cdots, x_N) = 0 \\ \vdots \\ f_N(x_1, x_2, \cdots, x_N) = 0 \end{cases} \qquad \textbf{(2.19)}$$

- Defining the correction value $\Delta X^{(t)}$ for each root vector $\hat{X}$ such that $F(\hat{X}) = 0$

$$\Delta X^{(t)} = \hat{X} - X^{(t)} \qquad \textbf{(2.20)}$$

- Expanding the N equations via the multivariate Taylor series and neglecting the higher order terms, we have the following equations:

$$\begin{cases} f_1(\hat{X}) = f_1(X) + \frac{\partial f_1(X)}{\partial x_1}\Delta x_1 + \frac{\partial f_1(X)}{\partial x_2}\Delta x_2 + \cdots + \frac{\partial f_1(X)}{\partial x_N}\Delta x_N + \cdots \\ f_2(\hat{X}) = f_2(X) + \frac{\partial f_2(X)}{\partial x_1}\Delta x_1 + \frac{\partial f_2(X)}{\partial x_2}\Delta x_2 + \cdots + \frac{\partial f_2(X)}{\partial x_N}\Delta x_N + \cdots \\ \vdots \\ \vdots \\ f_N(\hat{X}) = f_N(X) + \frac{\partial f_N(X)}{\partial x_1}\Delta x_1 + \frac{\partial f_N(X)}{\partial x_2}\Delta x_2 + \cdots + \frac{\partial f_N(X)}{\partial x_N}\Delta x_N + \cdots \end{cases} \qquad \textbf{(2.21)}$$

- **(2.21)** can be expressed in matrix form as follows:

$$\begin{bmatrix} f_1(\hat{X}) \\ f_2(\hat{X}) \\ \vdots \\ f_N(\hat{X}) \end{bmatrix} = \begin{bmatrix} f_1(X) \\ f_2(X) \\ \vdots \\ f_N(X) \end{bmatrix} + \begin{bmatrix} \frac{\partial f_1(X)}{\partial x_1} & \frac{\partial f_1(X)}{\partial x_2} & \cdots & \frac{\partial f_1(X)}{\partial x_N} \\ \frac{\partial f_2(X)}{\partial x_1} & \frac{\partial f_2(X)}{\partial x_2} & & \frac{\partial f_2(X)}{\partial x_N} \\ \vdots & \vdots & \ddots & \vdots \\ \frac{\partial f_N(X)}{\partial x_1} & \frac{\partial f_N(X)}{\partial x_2} & \cdots & \frac{\partial f_N(X)}{\partial x_N} \end{bmatrix} \begin{bmatrix} \Delta x_1 \\ \Delta x_2 \\ \vdots \\ \Delta x_N \end{bmatrix} \qquad \textbf{(2.22)}$$

- The N by N partial derivatives matrix is called the Jacobian matrix J(X)

$$J(X) = \begin{bmatrix} \frac{\partial f_1(X)}{\partial x_1} & \frac{\partial f_1(X)}{\partial x_2} & \cdots & \frac{\partial f_1(X)}{\partial x_N} \\ \frac{\partial f_2(X)}{\partial x_1} & \frac{\partial f_2(X)}{\partial x_2} & & \frac{\partial f_2(X)}{\partial x_N} \\ \vdots & \vdots & \ddots & \vdots \\ \frac{\partial f_N(X)}{\partial x_1} & \frac{\partial f_N(X)}{\partial x_2} & \cdots & \frac{\partial f_N(X)}{\partial x_N} \end{bmatrix} \qquad \textbf{(2.23)}$$

- **(2.22)** can be rewritten in simpler form:

$$F(\hat{X}) = F(X) + J(X).\Delta X = 0 \qquad \textbf{(2.24)}$$

- Deriving ΔX from **(2.24)** we get:

$$\Delta X = -J(X)^{-1}.F(X) \quad \textbf{(2.25)}$$

- Then, a new estimation is calculated:

$$X^{(t+1)} = X^{(t)} - J\left(X^{(t)}\right)^{-1}.F\left(X^{(t)}\right) \quad \textbf{(2.26)}$$

- With **(2.26)** solved in each iteration, $X^{(t+1)}$ gradually approaches the actual solution. Convergence can be evaluated by the norm of the correction value,

$$\left\|\Delta X^{(t)}\right\| < \varepsilon_1 \quad \textbf{(2.27)}$$

or by the norm of the function,

$$S_k = \left\|\Delta F(X^{(t)})\right\| < \varepsilon_2 \quad \textbf{(2.28)}$$

Hereε_1 and ε_2 are very small positive numbers specified beforehand.

ii. Newton Raphson Application to Power Flow

After resolving the power balance equation into real and imaginary part as it is shown in **(2.8)** and **(2.9)**,This separation produced a set of non-linear simultaneous NN equations in terms of the independent variables: voltage magnitude $|V_k|$in per unit, and phase angle δ_k in rad.

$$P_k^{(t)} = \sum_{n=1}^{N} \boldsymbol{Y}_{kn}\boldsymbol{V}_n^{(t)} \quad \boldsymbol{V}_k^{(t)} \cos\left(\delta_n^{(t)} + \theta_{kn}^{(t)} - \delta_k\right) \quad \textbf{(2.29)}$$

$$Q_k^{(t)} = -\sum_{n=1}^{N} \boldsymbol{Y}_{kn}\boldsymbol{V}_n^{(t)} \quad \boldsymbol{V}_k^{(t)} \sin\left(\delta_n^{(t)} + \theta_{kn}^{(t)} - \delta_k\right) \quad \textbf{(2.30)}$$

- Expressing the function and the variables in matrix form, we have:

$$X^{(t)} = \begin{bmatrix} \delta^{(t)} \\ V^{(t)} \end{bmatrix} \quad \textbf{(2.31)}$$

$$F(X^{(t)}) = \begin{bmatrix} P(X^{(t)}) \\ Q(X^{(t)}) \end{bmatrix} \quad \textbf{(2.32)}$$

$$C = \begin{bmatrix} P^{inj} \\ Q^{inj} \end{bmatrix} \quad \textbf{(2.33)}$$

- From **(2.24)** we can write:

$$\boldsymbol{C} = \boldsymbol{F}(X) + \boldsymbol{J}(X).\boldsymbol{\Delta}\mathrm{X}. \quad \textbf{(2.34)}$$

Or:

$$\boldsymbol{\Delta}\mathrm{X} = \frac{\boldsymbol{C} - \boldsymbol{F}(X)}{J(\boldsymbol{X})} \quad \textbf{(2.35)}$$

- Where $\boldsymbol{J}(X)$ is the Jacobian matrix of $\boldsymbol{F}(X)$

$$J(X) = \left[\begin{array}{ccc|ccc} \frac{\partial P_2}{\partial \delta_2} & \cdots & \frac{\partial P_2}{\partial \delta_N} & \frac{\partial P_2}{\partial V_2} & \cdots & \frac{\partial P_2}{\partial V_N} \\ \vdots & \ddots & \vdots & \vdots & \ddots & \vdots \\ \frac{\partial P_N}{\partial \delta_2} & \cdots & \frac{\partial P_N}{\partial \delta_N} & \frac{\partial P_N}{\partial V_2} & \cdots & \frac{\partial P_N}{\partial V_N} \\ \hline \frac{\partial Q_2}{\partial \delta_2} & \cdots & \frac{\partial Q_2}{\partial \delta_N} & \frac{\partial Q_2}{\partial V_2} & \cdots & \frac{\partial Q_2}{\partial V_N} \\ \vdots & \ddots & \vdots & \vdots & \ddots & \vdots \\ \frac{\partial Q_N}{\partial \delta_2} & \cdots & \frac{\partial Q_N}{\partial \delta_N} & \frac{\partial Q_N}{\partial V_2} & \cdots & \frac{\partial Q_N}{\partial V_N} \end{array}\right] \quad \textbf{(2.36)}$$

Or in simpler form:

$$J(X) = \begin{bmatrix} J_1 & J_2 \\ J_3 & J_4 \end{bmatrix} \quad \textbf{(2.37)}$$

- Jacobian matrix elements can be calculated using real and reactive power equations **(2.29)** and **(2.30)**, which are derived as follows:

a) The elements of J_1 are:

Diagonal:

$$\frac{\boldsymbol{\partial P_k}}{\boldsymbol{\partial \delta_k}} = \sum_{\substack{n=1, \\ n \neq k}}^{N} \boldsymbol{Y}_{kn} \boldsymbol{V}_n \boldsymbol{V}_k \sin(\delta_n + \theta_{kn} - \delta_K) \quad \textbf{(2.38)}$$

Off-diagonal:

$$\frac{\partial P_k}{\partial \delta_k} = -\boldsymbol{Y}_{kn} \boldsymbol{V}_n \boldsymbol{V}_k \sin(\delta_n + \theta_{kn} - \delta_K) \quad k \neq n \quad \textbf{(2.39)}$$

b) The elements of J_2 are:

Diagonal: $$\frac{\partial P_k}{\partial V_k} = 2\boldsymbol{Y}_{kk}\boldsymbol{V}_k\cos(\theta_{kk}) + \sum_{\substack{n=1,\\ n\neq k}}^{N} \boldsymbol{Y}_{kn}\boldsymbol{V}_n\cos(\delta_n + \theta_{kn} - \delta_K) \qquad \textbf{(2.40)}$$

Off-diagonal: $$\frac{\partial P_k}{\partial V_k} = \boldsymbol{Y}_{kn}\boldsymbol{V}_k\cos(\delta_n + \theta_{kn} - \delta_K) \quad k \neq n \qquad \textbf{(2.41)}$$

c) The elements of J_3 are:

Diagonal: $$\frac{\partial Q_k}{\partial \delta_k} = \sum_{\substack{n=1,\\ n\neq k}}^{N} \boldsymbol{Y}_{kn}\boldsymbol{V}_n\,\boldsymbol{V}_k\ \cos(\delta_n + \theta_{kn} - \delta_K) \qquad \textbf{(2.42)}$$

$\boldsymbol{i}$

Off-diagonal: $$\frac{\partial Q_k}{\partial \delta_k} = -\boldsymbol{Y}_{kn}\boldsymbol{V}_n\boldsymbol{V}_k\cos(\delta_n + \theta_{kn} - \delta_K) \quad k \neq n \qquad \textbf{(2.43)}$$

d) The elements of J_4 are:

Diagonal: $$\frac{\boldsymbol{\partial P_k}}{\boldsymbol{\partial V_k}} = -2\boldsymbol{Y}_{kn}\boldsymbol{V}_k\sin(\theta_{kk}) - \sum_{\substack{n=1,\\ n\neq k}}^{N} \boldsymbol{Y}_{kn}\boldsymbol{V}_n\sin(\delta_n + \theta_{kn} - \delta_K) \qquad \textbf{(2.44)}$$

Off-diagonal: $$\frac{\partial P_k}{\partial V_k} = -\boldsymbol{Y}_{kn}\boldsymbol{V}_k \quad \sin(\delta_n + \theta_{kn} - \delta_K) \quad k \neq n \qquad \textbf{(2.45)}$$

- The iteration calculation is started by providing an estimation of voltage magnitude and the initial voltage phase angle, usually we take the voltage magnitudes to be 1 per unit and the angles to be 0 rad.

$$X^{(0)} = \begin{bmatrix} {\delta_k}^{(0)} \\ {V_k}^{(0)} \end{bmatrix}$$

- The new estimation for the voltage magnitude and angle is:

$$X^{(t+1)} = X^{(t)} + \Delta X^{(t)} = \begin{bmatrix} {\delta_k}^{(t)} + \Delta{\delta_k}^{(t)} \\ {V_k}^{(t)} + \Delta{V_k}^{(t)} \end{bmatrix} \qquad \textbf{(2.46)}$$

- The changes in real and reactive power is reduced by real and reactive power calculated by the following equations:

$$\Delta P_i^{(t)} = \quad P_i^{inj} - P_i^{(t)} \qquad \textbf{(2.47)}$$

$$\Delta Q_i^{(t)} = \quad Q_i^{inj} - Q_i^{(t)} \tag{2.48}$$

- Convergence criteria are often based on $\Delta P_i^{(t)}$ and $\Delta Q_i^{(t)}$ (called power mismatches or the power residuals) rather than on $\Delta X^{(t)}$ (phase angle $\Delta \delta_k{}^{(t)}$ and voltage magnitude $\Delta V_k{}^{(t)}$ mismatches).[21]

$$\max\{\Delta P, \Delta Q\} < \varepsilon \tag{2.49}$$

iii. **Advantages and disadvantages of NR method**

a) Advantages:

- It possesses quadratic convergence and thus overall time for iterative process is short especially when the solution point is close.
- The region of convergence is large.
- It needs a smaller number of iterations to reach convergence.
- The number of iterations required in this method is almost independent of system size.
- It is not sensitive to the factors such like the initial estimations and slack bus selection.

b) Disadvantages:

- More calculations are involved in each iteration.
- The computation time per iteration is larger.
- It needs a larger computer memory requirement. The need of additional storage space since it involves calculation of Jacobian matrices
- Difficult solution method; the code is more complicated
- The solution can be more complicated if we face the case where the Jacobian matrix is singular matrix.

2.4.3. Fast Decoupled method

i. Basic concept

The Newton method was a landmark which, basically, comprises the repeated solution of a large set of linear equations. The strong convergence and the exploiting of the sparsity has made this method up to now the most general one in use. However, it was soon clear that the Jacobian was only necessary to obtain convergence and did not influence the final solution. One of the most extreme versions of such an approximated Newton method is the Fast-Decoupled Load flow (FDLD). [22]

The equations, from **(2.38**) to **(2.45**), are derived strictly from the mathematical viewpoint. It does not take the characteristics of power systems into consideration. Considering the later, the fast-decoupled method can be derived from the Newton method as it is discussed on the following:

- It is known that in high voltage power system the active power flow $\boldsymbol{P_k}$ is mainly related to the angle of the nodal voltage phasor $\boldsymbol{\delta_K}$, while reactive power flow $\boldsymbol{Q_k}$ is mainlyrelated to its magnitude $\boldsymbol{V}_k$.That makes the element of the Jacobian matrix:

$$J_2 = \frac{\partial P_k}{\partial V_k} \cong 0 \tag{2.50}$$

$$J_3 = \frac{\partial Q_k}{\partial \delta_K} \cong 0 \tag{2.51}$$

- So, the Jacobian matrix $J(X)$ will become

$$J(X) = \begin{bmatrix} J_1 & 0 \\ 0 & J_4 \end{bmatrix} \tag{2.52}$$

- To simplify the equations further, the analyzed power system must satisfy these conditions:
  - The R/X ratios are small for all branches.
  - The angle differences across the lines are small,$\delta_{Kn} \leq 20°(0.365\ rad)$.
  - The voltage magnitudes are close to their rated value,$V_k \cong 1\ p.u.$[23].
- Taking the above assumptions, the elements of $J_1$and J_4become as:

a) The elements of J_1 are:

Diagonal:

$$\frac{\boldsymbol{\partial P_k}}{\boldsymbol{\partial \delta_k}} = -|V_k| \quad B_{kk} \tag{2.53}$$

Off-diagonal:

$$\frac{\boldsymbol{\partial P_k}}{\boldsymbol{\partial \delta_k}} = -|V_k| \quad B_{kn};\ k \neq n \tag{2.54}$$

b) The elements of J_2 are:

Diagonal:
$$\frac{\partial \boldsymbol{Q_k}}{\partial \boldsymbol{V_k}} = -|V_k| \quad B_{kk} \tag{2.55}$$

Off-diagonal:
$$\frac{\partial \boldsymbol{Q_k}}{\partial \boldsymbol{V_k}} = -|V_k| \quad B_{kn};\ k \neq n \tag{2.56}$$

- The power mismatch vector can be decoupled:

$$\Delta \boldsymbol{P_k^{inj}} = \boldsymbol{J_1} \Delta \boldsymbol{\delta_k} = -|V_k| \sum_{n=2}^{N} B_{kn}{}' \Delta\delta_n \quad = -|V_k| \boldsymbol{B}' \Delta \boldsymbol{\delta_k} \tag{2.57}$$

$$\Delta \boldsymbol{Q_k^{inj}} = \boldsymbol{J_4} \Delta|\boldsymbol{V_k}| = -|V_k| \sum_{n=2}^{N} B_{kn}{}'' \Delta|V_k| \quad = -|V_k| \boldsymbol{B}'' \Delta \boldsymbol{\delta_k} \tag{2.58}$$

- $\boldsymbol{B'}$ and $\boldsymbol{B''}$ are two constant different dimensions matrices and they need to be formed once, they represent the imaginary part of the bus admittance matrix Y_{bus} where:
    - For N bus system, the dimension of $\boldsymbol{B'}$ is (N-1), it corresponds to all the busses except the slack bus.
    - And for M of PV busses, the dimension of $\boldsymbol{B''}$ is (N-1-M), it corresponds to all the busses except the slack bus and the PV busses.
- As a result, the iterative solution of the voltage magnitude changes and the angle variation is given by:

$$\Delta \boldsymbol{\delta_k}^{(t+1)} = -[\boldsymbol{B'}]^{-\boldsymbol{1}} * \frac{\Delta \boldsymbol{P_k^{inj\,(t)}}}{|V_k|^{(t)}} \tag{2.59}$$

$$\Delta|\boldsymbol{V_k}|^{(t+1)} = -[\boldsymbol{B''}]^{-\boldsymbol{1}} * \frac{\Delta \boldsymbol{Q_k^{inj\,(t)}}}{|V_k|^{(t)}} \tag{2.60}$$

- The new estimation for the voltage magnitude and angle is:

$$X^{(t+1)} = X^{(t)} + \Delta X^{(t)} = \begin{bmatrix} \delta_k{}^{(t)} + \Delta\delta_k{}^{(t)} \\ V_k{}^{(t)} + \Delta V_k{}^{(t)} \end{bmatrix} \tag{2.61}$$

- The power mismatch can be calculated:

$$\Delta P_i^{(t)} = \quad P_i^{inj} - P_i^{(t)} \tag{2.62}$$

$$\Delta Q_i^{(t)} = \quad Q_i^{inj} - Q_i^{(t)} \tag{2.63}$$

- The iterations stop when the condition **(2.49)** is satisfied:

$$\max\{\Delta P, \Delta Q\} < \varepsilon \quad \textbf{(2.49)}$$

ii. **Advantages and Disadvantages of FD**

a) Advantages

- Fast Decoupled method is the fastest of all methods, speed for FD iterations is nearly five times that of NR method. [23]
- It uses the characteristics of the power system which allow the omission of some of the computational process in iterative calculation, which greatly reduces the computational complexity. [24]
- The memory requirement is very less than the other methods like as Newton Raphson method, Gauss-Seidel method. [25]
- FD method more effective to bring out the precise reactive power losses which atrophied in between busses. [26]
- The FD method able to detect higher range of losses in large size of bus system. [26]

b) Disadvantages

- The convergence region decreases in size with the increasing of the ratio R/X; rendering the FD method does not work well on the distribution power networks which have high R/X ratio. [27]
- FD method takes more iterations than NR method to reach the solution within the same tolerance.
- The FD method is not appropriate for the computation of multiple solutions.
- The existing FDLF method requires more iterations to converge

2.5. Conclusion

This chapter presents different solutions conventional methods the power flow analysis. Newton Raphson technique is the most used conventional method so that it works well for network operating near nominal load conditions but has poor performance for networks under heavily loaded conditions. The presented methods in this chapter are unable to cope with the islanded MGs. Therefore, unconventional methods were developed to deal with MGs problems like a droop control with Newton Raphson concept which will be presented in the next chapter.

Chapter 3

Power Flow Analysis for Islanded Microgrid

3.1. Introduction

For steady-state studies of isolated operating mode MG, an accurate, fast, scalable, efficient power flow analysis tool is crucial. Conventional power flow analysis face challenges when applied to isolated microgrids such as singularity results from system radiology, high R/X ratio, relatively small rated distributed generation (DG) units and thus absence of conventional slack bus, extensive computational burden, convergence issues and extensive solution time. Although branch-based power flow techniques are more preferred for distribution systems to overcome some of the aforementioned challenges, these techniques are incompatible with isolated microgrids as they necessitate the availability of a slack bus, therefore simplified algorithms are proposed such that the voltage of slack bus and the frequency of the MG are determined by the operating conditions of the MG loads and DG units and they are controlled by the corresponding droop characteristics. [28]

3.2. Droop Control Method

The communication-based control systems are most suitable in centralized systems like an electrified aircraft. However, the application like DC microgrids where the loads and the power converters are connected at a common point popularly termed as the point of common coupling, demands an economical and reliable control framework. The communication-based systems are less likely suitable for microgrid application due to the cost involved in using high bandwidth communication network and data reliability. The droop control strategy holds an edge over the other control strategies due to the fact that no communication among the power converters is required. Thereby the reliability is improved without any restriction on the physical location of the power converters tied to the distributed generators. The droop strategy is most widely preferred since it facilitates to investigate the performance parameters of the system like voltage regulation, Total harmonic distortion (THD), Load-sharing and stability in a microgrid. [29] This control method is usually implemented on the conventional power plants to control the injected power of synchronous generators to the grid. Also, droop control has been used to control the active and reactive power of distributed generations in microgrids. Frequency and voltage control of microgrid and proper power sharing between DGs are the most important goals of droop control in the islanded mode of operation. [30]

For AC microgrid application, the output of the power converters is destined to be AC. The possible power converter for the system could be of either DC to AC converter popularly known as inverters or AC to AC converters. Since most of the power sources are predominantly DC, the droop control of parallel inverters is presented in the literature survey of this section. [29]

Droop methods are based on the behavior of synchronous generators. The equivalent circuit of a synchronous generator connected to the grid is presented in **Figure 3.1** the real power injected into the grid can be expressed as:

$$S=P+jQ \quad \textbf{(3.1)}$$

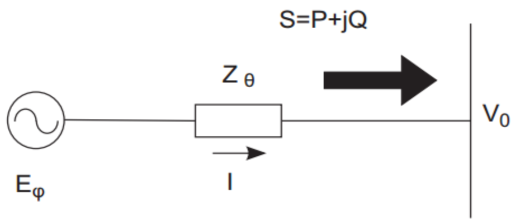

Figure 3.1 Synchronous generator connected to an AC bus.

Where P and Q are the active and reactive powers. An impedance, Zy, is shown between the grid and the generator in **Figure 3.1**. This impedance is formed by the synchronous or internal impedance of the generator and the line impedance existing between the generator and the grid. On the one hand, the internal impedance presents a mainly inductive behavior.

These generators are usually connected to high voltage lines, which are also mainly inductive. Consequently, the impedance of the equivalent circuit is considered inductive and the active and reactive powers can be described as follows:

$$P = \frac{EV}{X}\, sin\emptyset \quad \textbf{(3.2)}$$

$$Q = \frac{EV\, cos\emptyset - V^2}{X} \quad \textbf{(3.3)}$$

From **(3.2)** and **(3.3)**, taking into consideration small phase differences between E and V ($\sin\emptyset \approx \emptyset$ and $\cos\emptyset \approx 1$), it is observed that P and Q depend mainly on f and E–V, respectively. In this way, P and Q can be controlled by means of the phase and amplitude of the output voltage, respectively. Consequently, thanks to the fact that the inductive behavior of the synchronous impedance P and Q influences the voltage and frequency of the generated voltage, respectively and benefits synchronous behavior when two or more generators work in parallel. Taking all these factors into account, the reproduction of this behavior in power converters is proposed in. The simplest way of reproducing this behavior in the power converters is to add the characteristics shown in **Figure 3.1** explained by the equations **(3.4)** and **(3.5)** [31]. Taking into account that the converter output impedance is considered to be inductive due to the high inductive component of the line impedance and the large inductor filter (1 mH), we may assume that the line is mainly inductive (X>>>R) the resistive part can be neglected in addition to that the power angle in such lines is small ($\sin\emptyset \approx \emptyset$ and $\cos\emptyset \approx 1$).

Depending upon the drooping characteristics, the droop control strategies are classified into linear and nonlinear droop. The classification of linear droop strategy is as shown in **Figure 3.2**. [29]

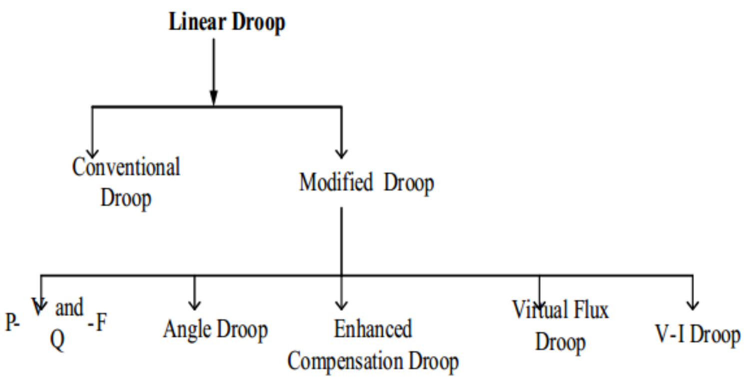

Figure 3.2 Droop control strategy classification

The linear droop can further be classified into conventional droop and modified droop. Linear droop control aims at generating a proper reference based upon the droop in parameters like frequency, voltage, power angle.

The main advantages and drawbacks of the conventional droop control are presented in **Table 3.1**. In order to overcome these disadvantages, a couple of proposed variations are demonstrated.

- Load sharing and voltage and frequency regulation trade-off

One of the drawbacks described in **Table 3.1** is the inherent trade-off of the droop method between voltage regulation and load sharing. The main solutions proposed can be classified in restoration controls, dynamic slopes and high gain angle droop control instead of frequency droop control.

Table 3.1 Advantages and disadvantages of droop control **[**32**]**

Advantages	**Disadvantages**
No communication Great Flexibility High readability Free laying Different power rating	Trade-off between voltage regulation and load sharing poor harmonic sharing coupling inductances influence of system impedance slow dynamic response

- Harmonic load sharing

The original droop method guarantees good P and Q sharing but does not take into account harmonic load sharing in the case of nonlinear loads. The main proposals are the addition of a loop that reduces the gain and bandwidth of the reference voltage in the presence of distorted components to the droop control, injection of an AC signal, virtual impedance, harmonic droop coefficients and cooperative harmonic filtering strategy.

- Coupling inductances

These components increase the size and weight of the system. These physical inductances can be replaced by virtual impedance and consecutive virtual impedance variations.

- Line impedance.

The line impedance between the paralleled converters also affects the performance of the original droop method. Several techniques have been proposed in order to overcome this drawback: additional loop with grid parameters estimation, voltage droop coefficient by means of output active and reactive powers, decoupling of P and Q, reactive current addition to the droop control loop and estimation of the impedance voltage drops.

- Dynamic response

The original droop method presents a slow, oscillating dynamic response which is overcome in several proposed solutions: angle droop instead of frequency droop, adaptive decentralized droop , droop based on coupling filter parameters, droop based on H1, derived from linear matrix inequality (LMI), control theory and addition of derivative terms.

- Integration of renewable energy resources

Finally, the last drawback of the original droop method is its poor performance with renewable energy resources. In order to mitigate this, a nonlinear droop control is proposed in and a hybrid maximum power point tracking (MPPT) with droop control. [29]

3.2 Droop Control with Newton Raphson

One way for solving power flow analysis of islanded MG is by using the NR method with the droop control method taking into account the droop characteristics of the DGs. A slack bus is considered to be connected at a random MG node. The operational conditions of this slack bus as well as of the rest MG nodes are determined through an iterative procedure. The objective of this procedure is to force the active and reactive power flowing through the slack bus to zero, representing the islanded MG operation. The proposed approach has a similar accuracy with time-domain simulations, while it reduces significantly the required computational burden. [33]

- **Y_{bus} Model**

Since the system frequency is not constant in an islanded microgrid, the Y_{bus} is also not constant because the reactance in the Y_{bus} depends on the frequency Therefore, for a system with N buses, Y_{bus} will be a function of the system frequency as follows:

$$Y_{bus}(f) = \begin{bmatrix} Y_{11}(f) & Y_{12}(f) & \cdots & Y_{1j}(f) & \dots & Y_{1n}(f) \\ Y_{21}(f) & Y_{22}(f) & \cdots & Y_{2j}(f) & \dots & Y_{2n}(f) \\ \vdots & \vdots & \vdots & \vdots & \vdots & \vdots \\ Y_{k1}(f) & Y_{k2}(f) & \dots & Y_{kj}(f) & \dots & Y_{kn}(f) \\ \vdots & \vdots & \vdots & \vdots & \vdots & \vdots \\ Y_{n1}(f) & Y_{n2}(f) & \dots & Y_{nj}(f) & \dots & Y_{nn}(f) \end{bmatrix} \quad \textbf{(3.1)}$$

Where: $$Y_{bus}(f) = \begin{cases} -y_{kn}(f) & k \neq n \\ \sum_{\substack{k=1 \\ k\neq n}}^{N} y_{kn}(f) & k = n \end{cases} \quad (3.2)$$

$$Z_{kn} = R_{kn} + jX_{kn} \quad (3.3)$$

- **Distributed generator model**

In grid connected mode, DGs are usually modeled as PV or PQ buses. In islanded mode, since there is no slack bus, it is impossible to model all the DGs as PV or PQ buses. So DGs in islanded microgrids are modeled as droop buses where the voltage and the frequency droop controls are based on the well known active power-frequency (P/f) and reactive power-voltage (Q/V) droop characteristics as it is shown in **Figure 3.3**.

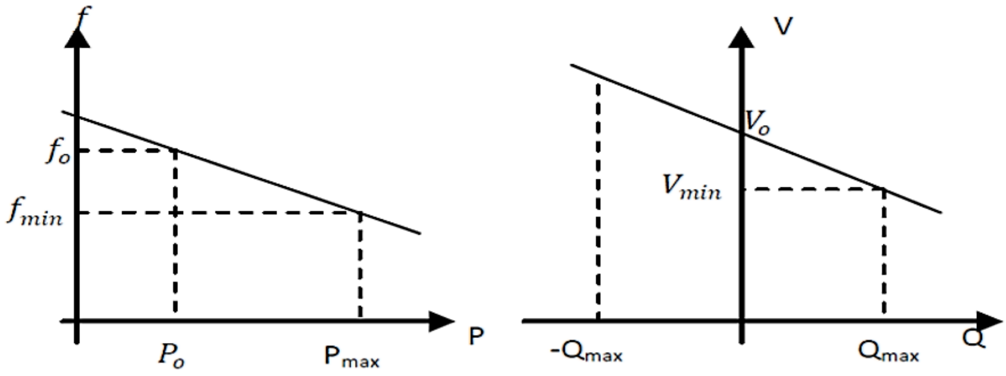

Figure 3.3 P/ f and Q/ V Droop Characteristics of a DG

The single line control diagram of conventional droop is represented in **Figure 3.4**.

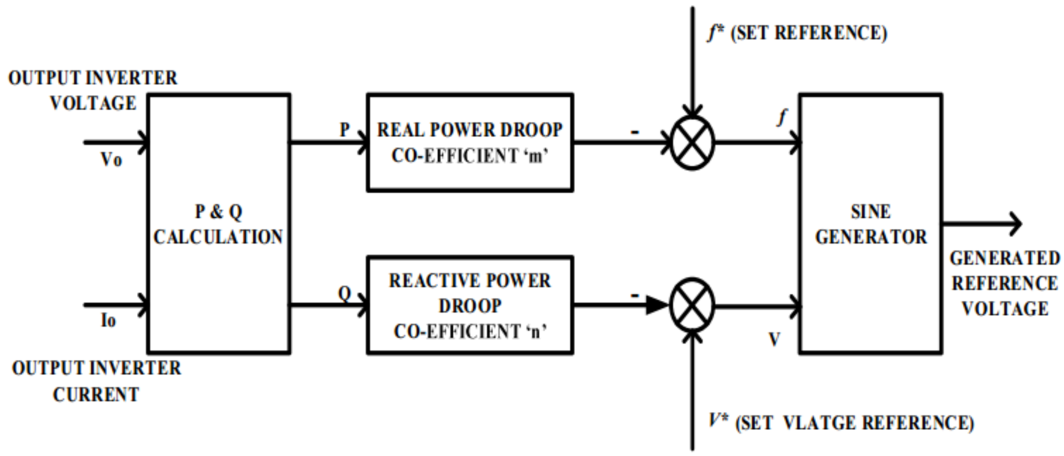

Figure 3.4 Conventional droop control scheme

The DG units in an islanded MG operate using the droop control, where the operating MG frequency f_{grid} and the voltage magnitude Vi at the output of the i-th DG unit are determined by the following equations:

$$f_{grid} = f_{max} - m_i p_i \qquad \forall\, i \in N_{dg} \qquad \textbf{(3. 4)}$$

$$V_i = V_{max} - n_i Q_i \qquad \forall\, i \in N_{dg} \qquad \textbf{(3.5)}$$

Such that:

$$m_i = \frac{f_{max} - f_{min}}{p_{max,i}} \qquad \forall i \in N_{Dg} \qquad \textbf{(3.6)}$$

$$n_i = \frac{V_{max} - V_{min}}{Qmax_i} \qquad \forall i \in N_{Dg} \qquad \textbf{(3.7)}$$

Where N_{dg} denotes the number of the installed DG units. V_{max}, V_{min}, f_{max} and f_{min} are the maximum and minimum operational limits of voltage and frequency, respectively. Additionally, Q_{max},i is the maximum available reactive power of the i-th DG unit P_i and Qi are the injected active and reactive power of the i-$_{th}$ unit, respectively. m_i and n_i are the corresponding droop coefficients.

For several DG units connected in parallel constituting a microgrid, the load power sharing depends on the slope of the droop characteristics. The main idea is that when there is an increase in the load, the frequency reference is decreased. Similarly, reactive power is shared using the droop characteristic of the voltage magnitude.

3.3 Conclusion

This chapter provides background information about new methods used for calculating the power flow analysis (PFA) upon which this research is built. It revisits non-conventional power flow analysis method droop control, such that it is suitable for networked islanded microgrids. The theories and the equations are stated in order to apply them in the next chapter.

Chapter 4

Simulation Results and Discussion

4.1. Introduction

Power flow analysis methods are widely used in transmission and distribution networks, however a lot of them are complicated and not easy to implement. This chapter attempts to construct an islanded microgrid Power flow computer program that is the basic tool for investigating a Successful power system operation under normal balanced three phase steady-date conditions. This program computes voltage magnitude and angle at each bus, in autonomous microgrid power system (PS) under steady state operation. It computes also P, Q for all equipments interconnecting the buses, for this purpose, more simplified algorithms are proposed and developed to get better results.

4.2. Newton Raphson with Droop Control Method

This section presents a methodology for the steady state analysis, i.e., power flow analysis, of islanded AC microgrids, operated under the droop control scheme. In the proposed framework, the power flow is computed using conventional power flow methods. For this purpose, a slack bus is considered to be connected to a random node of the examined MG. Subsequently, an iterative procedure is applied to determine the operational conditions, i.e., voltage level, frequency, active and reactive power absorption/injection, of this slack bus as well as of the rest MG nodes. The objective of the proposed iterative procedure is to force active and reactive power, flowing through the slack bus, to zero, emulating this way the islanded operation of the MG. The flowchart of this methodology is shown in **Figure 4.1**. [3]

4.2.1. Seven Bus Microgrid Simulation

For performing power flow analysis, two algorithms are proposed and validated in order to improve the system power flow behavior.

4.2.1.1 First Algorithm Structure

The proposed iterative method flowchart is shown in **Figure 4.1** and it consists of the following steps:

Step1: The initial conditions are applied. In particular, V_{sb} which is the slack bus voltage and f_{grid} which is the grid frequency receive the maximum permissible values, i.e. V_{max} and f_{max}, respectively. Additionally, variables V_{ub} and V_{lb} are set equal to V_{max} and V_{min}, respectively. A further insight on these variables will be given in step7. For the initialization, the active power injections of all DG units are considered equal to zero, while reactive power injections are considered equal to $-Q_{max,i}$. In each power flow calculation, active and reactive power injections are stored in two discrete vectors denoted for the rest of the paper as $\mathbf{P_{dg}}$ and $\mathbf{Q_{dg}}$, respectively. Finally, at this step, the user defines the maximum number of iterations, i.e., *MaxIter*, and the tolerances for the convergence of the three loops, i.e. *tolp, tolv, tolq*.

Step2: Using the initial value of the frequency f_{grid} given by step 1 and the lines data, the admittance matrix is built.

Denoting that: the element in row i, column j where i,j ϵ N*

-the matrix is symmetric so: $Y_{ij}=Y_{ji}$ **(4.1)**

-the diagonal elements are obtained such that: $Y_{ii} = Y_{i0} + \sum_{\substack{j=1 \\ j\neq j}}^{N} Y_{iN}$ **(4.2)**

-the off diagonal elements are: $Y_{ij}= -Y_{ji}$ **(4.3)**

Such that $y_{i0} = \frac{1}{Z_{i0}}$ **(4.4)**

And $Z_i = R_i + j2\pi fL$ **(4.6)**

Step3: The power flow analysis of the network is performed using the two previous steps and the Newton-Raphson equations given in the section **(2.4.2)**. This power flow aims to calculate network voltages and the active power flowing through the slack bus (*Psb*). The iteration calculation is started by providing an estimation of voltage magnitude and the initial voltage phase angle. In this algorithm the voltage magnitudes is set to be 1 per unit and the angles to 0 rad. The type of the buses and their injected power should be specified. In this work the slack bus is chosen to be at bus five, moreover the type of the all buses is selected to be PQ buses, as it is shown in **Table 4.2**. After that the power mismatch at each bus is calculated by comparing the power computed using the two power balance equations **(2.29)** and **(2.30)** ,and the injected powers .the convergence will be achieved whenever the mismatch is less than some tolerance value specified means: $\max\{\Delta P, \Delta Q\} < \varepsilon$ hence ,voltages and angles of busses would result and the algorithm moves to next step, otherwise the voltages and angles will be updated by means of the Jacobian matrix and new mismatched will be obtained. After that the active power flowing through the slack bus (P_{sb}) is calculated using the active power balance equation.

Step4: In this step a convergence check is performed to evaluate if the absolute value of P_{sb}, i.e., $|P_{sb}|$, is greater than the predefined tolerance *tolp*. If so, P_{sb} must be reallocated to all installed DG units in order to zero the active power flowing through the slack bus. To achieve this objective, all DG units must adjust their injected active power by a ΔP_i amount. This amount can be mathematically expressed using the following equations:

$$\sum_{i=1}^{N_{Dg}} \Delta Pi = P_{Sb} \qquad \forall i \in N_{Dg} \tag{4.7}$$

$$m_1 \Delta P_1 = \cdots m N_{Dg} \Delta P_{N_{Dg}} \forall i \in N_{Dg} \tag{4.8}$$

then, P_{dg} which is the vector of active power injections of DG units is updated by adding the corresponding ΔP_i amounts. Subsequently, the new f_{grid} is calculated using the equation **(3.4)**.

After that, the procedure moves back to Step 2. Then, a new power flow is performed using the updated values of P_{dg} and f_{grid}. When |Psb| becomes lower than *tolp*, the algorithm moves to Step5.

Step5: Reactive power injections of all DG units, i.e., $\boldsymbol{Q}_{dg}$ are computed according to equation **(3.5)**.

Step6: Voltages of all MG nodes are computed through a power flow analysis using P_{dg}, Q, and f_{grid}. A similar process of power flow will be repeated as in step 3 until voltages and angles results. Using the results of the last power flow, the reactive power flowing through the slack bus, i.e., $Q_{sb,}$ is calculated.

Step7: If the absolute value of Q_{sb}, i.e. $|Q_{sb}|$, is less than *tolq*, the algorithm moves to Step8 and terminates, this means that the calculations are done and the final values of the frequency, the generated active and reactive power, the voltages and phase angles are the desired values for the islanded microgrid load flow solution. Otherwise, we must update the slack bus voltage so that it was the reference that does not change during all the previous steps therefore, a new V_{sb} must be defined to zero the reactive power flowing through it. More specifically, a negative Q_{sb} value indicates a surplus of reactive power in the MG, absorbed from the slack bus. Therefore, according to equation **(3.5)**, V_{sb} must be increased to force DG units to reduce their reactive power injection. On the contrary, if Q_{sb} is positive, V_{sb} must be reduced. The new value of V_{sb} is determined through a binary search method. The binary search algorithm is presented in **Algorithm 1**. Where, V_{ub} and V_{lb} are the upper and lower limits of the searching interval, while p and$n$ are the corresponding previous and new values. Once the new V_{sb} is defined, the procedure moves back to step2.

Step8: The procedure terminates providing the power flow solution of the examined MG.

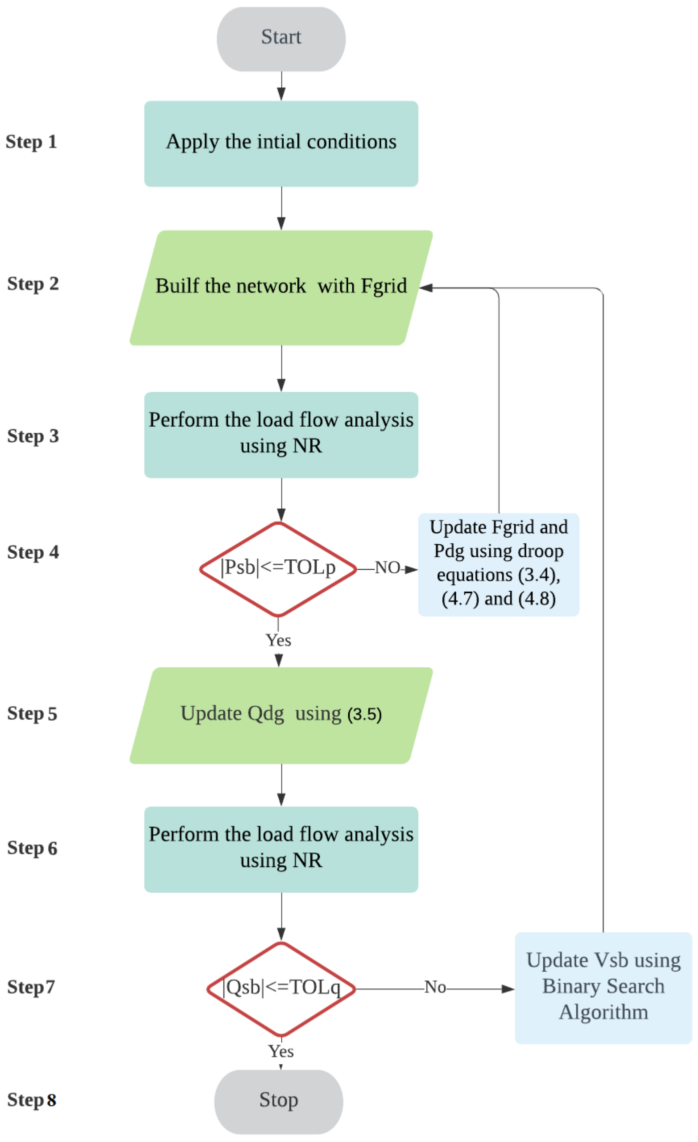

Figure 4.1 flowchart of the first method

Algorithm 1:

if $Q_{Sb}>0$ then
  set $V_{Sb}= V_{Sb}-(V_{Sb}- V_{LB})/2$
  and $V_{UB} =V_{Sb}$
else
  set $V_{Sb}= V_{Sb}+(V_{Sb}- V_{LB})/2$
  and $V_{UB} =V_{Sb}$
end

4.2.1.2 Validation of the First Algorithm

- To validate the proposed power flow approach, the previous method is applied to 0.4 kV islanded MG demonstrated on a 7 bus system (shown in **Figure 4.2**) and simulated using MATLAB R2015a.
- The network consisting of seven buses, two of them are load buses constant power (CP) and constant impendence (CZ) loads and three DG units chosen to be PQ buses as specification of their types. In grid connected mode, DGs are usually modeled as PV or PQ buses, however in islanded mode, since there is no slack bus; DGs are modeled as droop buses.
- The well defined types of buses in the literature are slack, PV and PQ buses. The selection of bus depends upon the pre-specified quantities. In general, any bus can be a reference bus. In our circuit the slack bus is randomly selected on bus 5.
- The nominal power factor of the DG units is 0.85 while the loads operate with inductive power factor equal to 0.95.
- The entire network elements are operating at their nominal value and the time domain calculation are provided in [33].

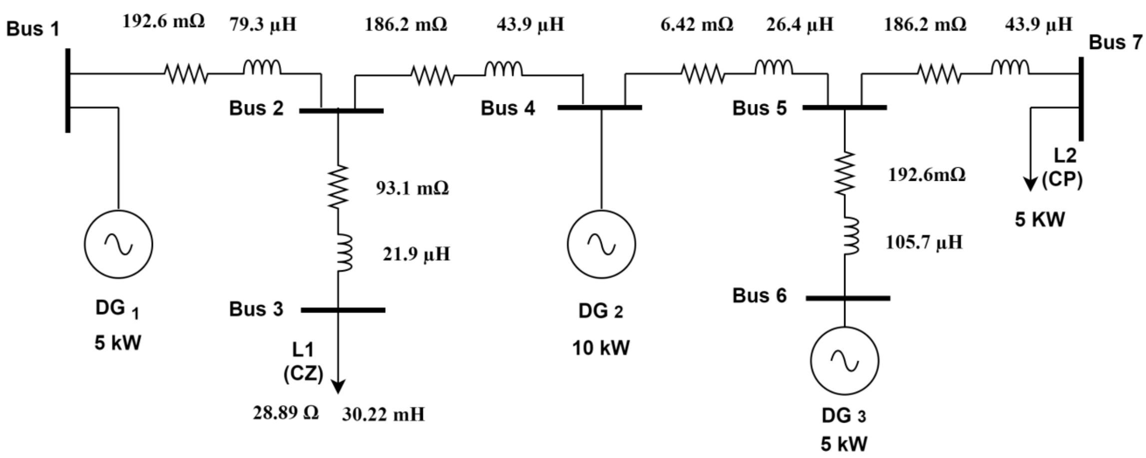

Figure 4.2 Seven bus test system

The initial values used for testing the proposed network are resumed in the following tables.

Table 4.1 The initial values of the 7 bus proposed network

Initial Conditions				
Variables	**P_i (KW)**	**Q_i (VAR)**	**V_i**	**δ_i**
Values	Pl(7) = 5	▪ For DG units buses: $Qi = -Q_{max,i} = -P_{maxi} * \tan(\cos 0.85).$ ▪ For load buses: $Q7 = 5000 * 0.95 = 4750.$ ▪ Other buses : $Qi = 0.$	440	0

Droop coefficients	**m (Hz/Kw)**			**n (V/KVAR)**		
	m_1	**m_2**	**m_3**	**n_1**	**n_2**	**n_3**
Values	0.400	0.200	0.400	12.924	6.462	12.924

Binary Search Algorithm						
Variables	**V_{max}**	**V_{ub}**	**V_{lb}**	**Tol_p**	**Tol_q**	**f (Hz)**
Values	440	440	360	0.01	0.01	51

Table 4.2 The proposed network bus classification

The bus number	The bus type
1	Generated bus (PQ)
2	Generated bus (PQ)
3	Load bus (PQ)
4	Generated bus (PQ)
5	Slack bus
6	Generated bus (PQ)
7	Load bus (PQ)

The proposed algorithm of **Figure 4.1** was developed in the MATLAB environment to solve the power flow problem of the islanded microgrid shown in **Figure 4.2** using the data demonstrated on the table 4.1 the following results are obtained:

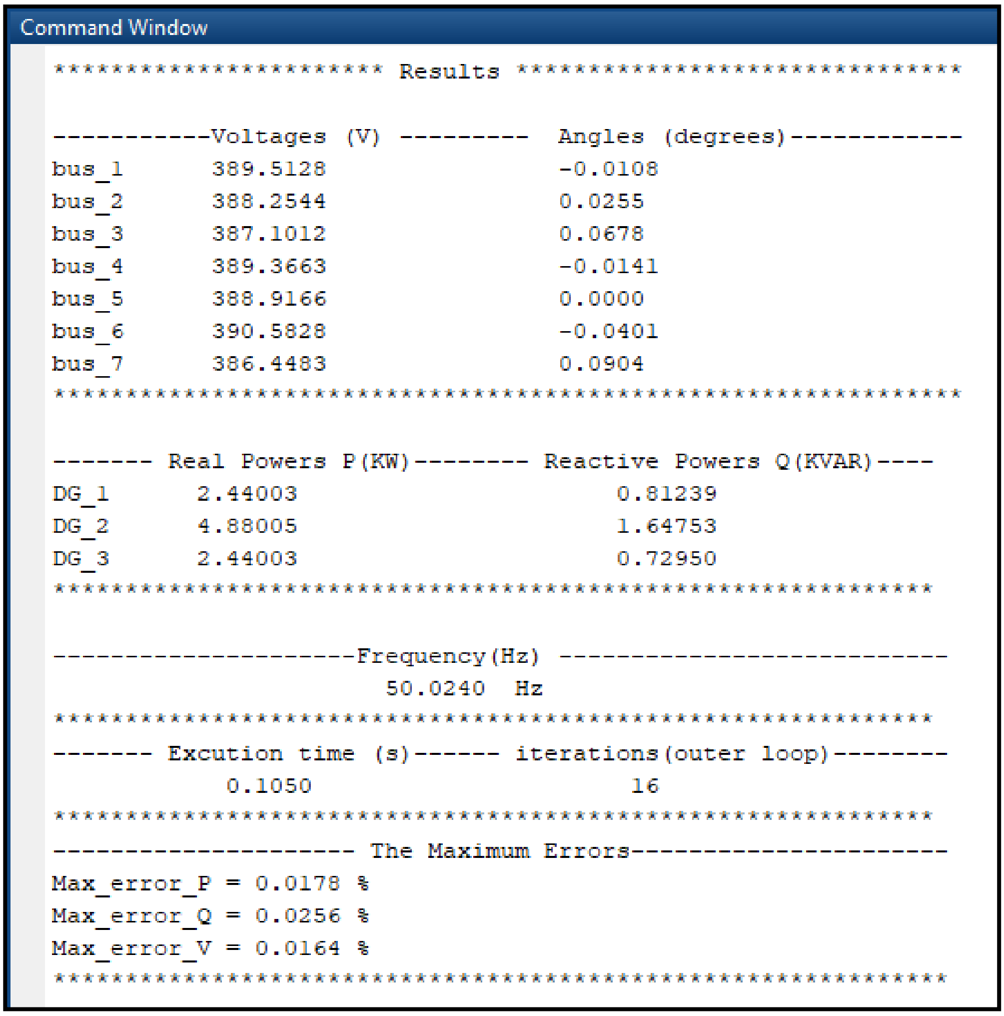

```
Command Window
*********************** Results *******************************

-----------Voltages (V) ---------  Angles (degrees)------------
bus_1      389.5128                -0.0108
bus_2      388.2544                0.0255
bus_3      387.1012                0.0678
bus_4      389.3663                -0.0141
bus_5      388.9166                0.0000
bus_6      390.5828                -0.0401
bus_7      386.4483                0.0904
***************************************************************

------- Real Powers P(KW)-------- Reactive Powers Q(KVAR)----
DG_1      2.44003                      0.81239
DG_2      4.88005                      1.64753
DG_3      2.44003                      0.72950
*************************************************************

---------------------Frequency(Hz) --------------------------
                    50.0240  Hz
*************************************************************
------- Excution time (s)------ iterations(outer loop)--------
            0.1050                       16
*************************************************************
--------------------- The Maximum Errors----------------------
Max_error_P = 0.0178 %
Max_error_Q = 0.0256 %
Max_error_V = 0.0164 %
**************************************************************
```

Figure 4.3 Results of the proposed algorithm.

The voltages, active and reactive power of the network performed by PSIM software and our proposed algorithm are shown in **Table 4.3**.

Table 4.3 table of network steady-state voltages, active, and reactive power of DG units

Network Bus Voltages (V)							
Bus	**1**	**2**	**3**	**4**	**5**	**6**	**7**
PSIM	389.575	388.315	387.162	389.429	388.978	390.647	386.507
Proposed	389.513	388.254	387.101	389.366	388.916	390.583	386.448

	Real Power P (KW)			Reactive Power Q(KVAR)		
Powers	**P_1**	**P_2**	**P_3**	**Q_1**	**Q_2**	**Q_3**
PSIM	2.44046	4.88086	2.44046	0.81238	1.64756	0.72951
Proposed	2.44003	4.88005	2.44003	0.81239	1.64753	0.72950

➢ Comparison

- Time domain (TD) simulations in [33] are performed using PSIM software. All their simulations are performed using an Intel Core i7-930, 2.8 GHz, RAM 24 GB, personal computer. Our algorithm is validated using Intel Core i3-311M, 2.4 GHz, RAM 4 GB, personal computer.

- For our algorithm validation MATLAB is utilized for the modeling of the developed control schemes and especially the incorporation of droop control for the injected active power of each DG unit.

-The simulation time of our MATLAB code is **0.1050** which is a remarkable value compared to that of the paper [33]in which their algorithm converges at 2.065s, and this is due to the fact that we have developed MATLAB code without an interface with other software, whereas in [33] the openDSS is utilized as a phase-domain power flow solver, employing phase-domain analysis of the network, this latter delays the time of conversion considerably. Therefore we conclude that our proposed method is more efficient in terms of convergence time reduction.

- One can see that the error in active and reactive power as well as the voltages is so negligible, this latter proof the advantage of our algorithm for getting better results.

-The droop equation for the voltage of the DGs (2) in [33]is not practical so that Q_{max} should be removed in order to get good results. The general equations for connected MG are:

$$f = f_0 - m_p(P_G - P_0) \quad \textbf{(4.9)}$$

$$V = V_0 - n_p(Q_G - Q_0) \quad \textbf{(4.10)}$$

P_o and Q_o are the active and reactive power set points, respectively; and are normally set to zero when dealing with islanded operation of MG which is our case of study. [34]

-The initial conditions changes don't really affect the results too much.

- Our algorithm was similarly performed in [35]. The results of our proposed algorithm are more accurate and more close to the time domain simulation compared to [35]. The key concept used in [35] is that each time of performing PFA, the initial conditions was changed for obtaining the closest possible result values to that in [33], and this is not satisfying the algorithm which we follow.

-We can remark on the network shown in **Figure 4.2** that the line impedances should be multiplied by 10 in order to fit the values in [33]. Therefore, it can be concluded that our proposed method is a valuable tool for distribution system operators for close to real-time simulations of islanded MGs.

The DGs active power, reactive power and the frequency are plotted as follow:

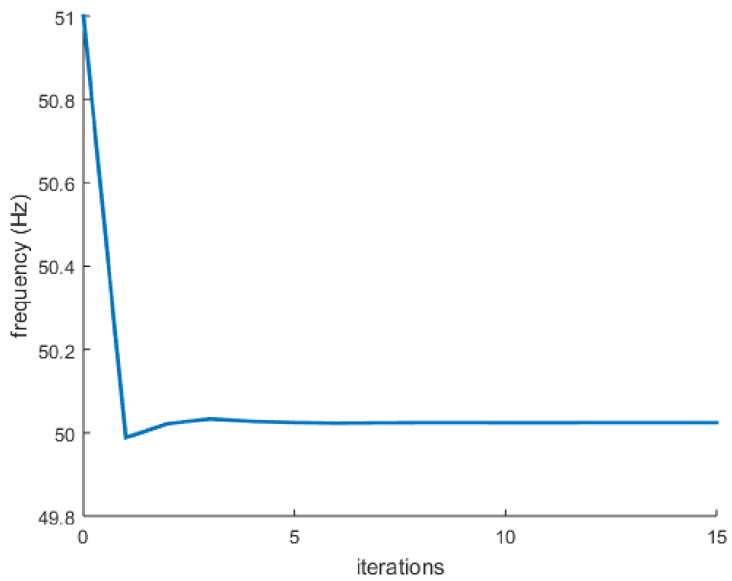

Figure 4.4 Variation of grid frequency with respect to the iteration

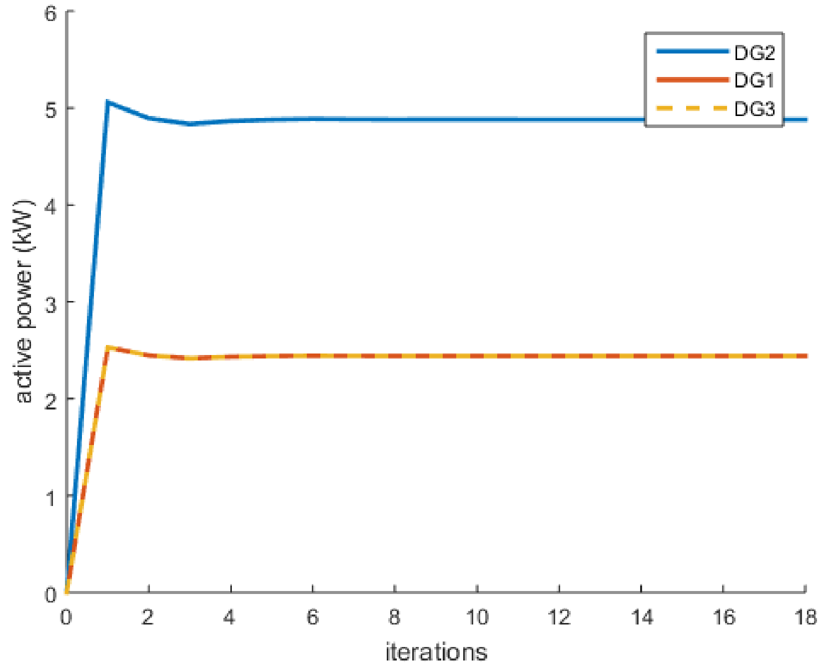

Figure 4.5 Variation of active power with respect to the iteration

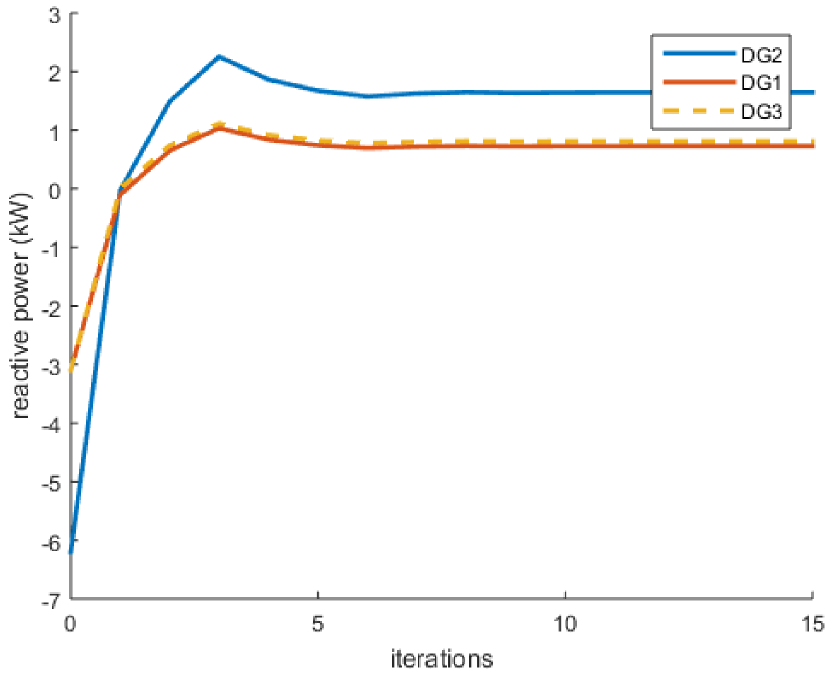

Figure 4.6 Variation of reactive power with respect to the iteration

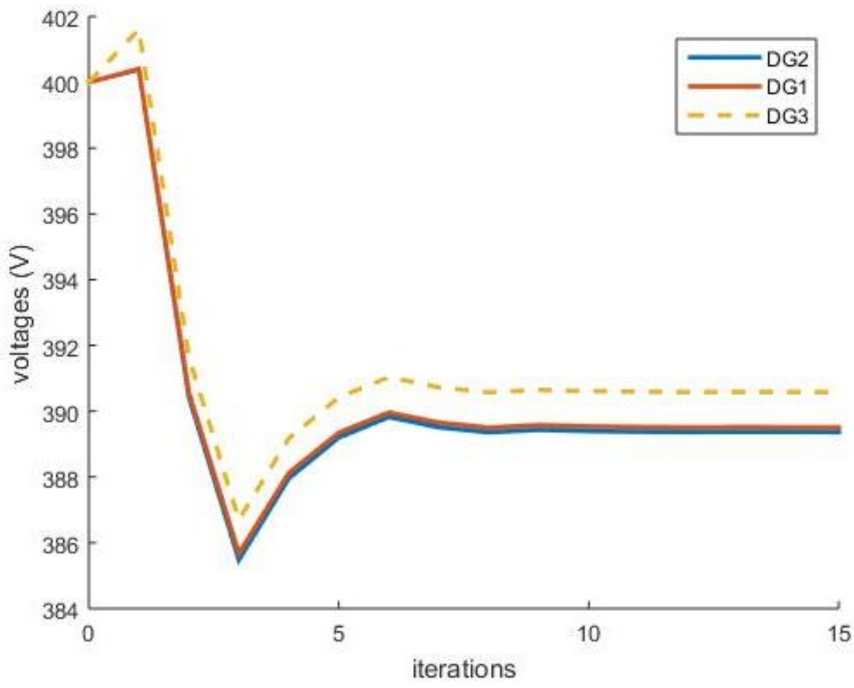

Figure 4.7 Variation of voltage with respect to the iteration

- **Discussion**

For the first graph **(Figure 4.4)** we could notice that the frequency of the network starts from 51Hz which is the initial value stated on the algorithm, along with the iterations the frequency decreases gradually as the DGs active power increases, and this satisfies the equation **(3.4)**. The frequency stabilizes finally at 50.024Hz after some number of iterations as it is checked in **Figure 4.3**.

For the second graph **(Figure 4.5)**, active power DGs of the microgrid is displayed. we can remark that the active power start from zero as it is the initialization value in our algorithm and it start increasing gradually along with the iterations satisfying the droop equation **(3.4)**. DG1 and DG3 are identical. After some number of iterations, the steady state is reached and the final active power for the DGs is shown in **Figure 4.3**.

For the third graph **(Figure 4.6)**, reactive power DGs of the microgrid is displayed. we can remark that the reactive power start from some value $-Q_{max}$ for each DG so that it is the initialization value in our algorithm and it start increasing gradually along with the iterations satisfying the droop equation **(3.5)**. After some number of iterations, the steady state is reached and the final reactive power for the DGs is shown in **Figure 4.3**.

In the fourth graph **(Figure 4.7)**, DGs voltage is displayed. It starts from the maximum initial value and until steady state convergence after a number of iterations. This graph demonstrates the results shown in **Figure 4.3** with a minimum value 386.44V at bus 7.

4.2.1.3 Second Algorithm structure

This section presents an extended methodology for performing PFA, operated under the droop control scheme applied on the same network of the previous section.

The previous work has given good results however, modeling of voltage dependent droop curves using iterative procedures, may result in numerical oscillations of the injected power and network voltages. As discussed in [36] and [37], in extended networks with high penetration of DG units, these spurious oscillations may lead to convergence issues. Therefore, in these cases, the method of [33] may fail to provide consistent results. To overcome this issue, in this section, the previous method is further extended to enhance the power flow analysis of largescale islanded MGs. Towards this objective, a third loop is added. The aim of this loop is to simulate with higher accuracy the $Q - V$ droop control. [3]

The objective of the proposed iterative procedure is similar to what is introduced before which is to force active and reactive power, flowing through the slack bus, to zero, emulating this way the islanded operation of the MG. The flowchart of this methodology is shown in **Figure 4.8**.

The proposed methodology consists of three nested loops, as presented in **Figure4.8.** The inner loop is used to calculate f_{grid}, while the outer loop defines V_{sb}, and the additional loop defines the injected reactive power for eliminating the oscillations.

Step1: The initial conditions are applied as in the previous section. Additionally, at this step, the user defines the value of the integral term k, used to calculate reactive power injections of DG units. A further insight on this integral term is provided in step8. Finally, at this step, the user defines the maximum number of iterations, i.e., *MaxIter*, and the tolerances for the convergence of the three loops, i.e. *tolp*, *tolv*, *tolq*.

Step2: Using the initial value of the frequency f_{grid} given by step 1 and the lines data, the admittance matrix is built.

Step3: The power flow analysis of the network is performed using the two previous steps and the Newton-Raphson equations given in the section **(2.4.2)**. The value of counter c is set to 1. This counter is used to monitor the number of iterations performed during the second loop of the proposed algorithm. Further information concerning this counter can be found in steps 5 to 10. After that the active power flowing through the slack bus (P_{sb}) as well as the network voltages (V^c) are computed.

Step4: From step 3, the injected power of slack bus is checked if it is less the active power tolerance given by step 1. In case of the injected power of the slack bus is greater than *Tolp* the generated active power of the DGs is updated using the equations **(4.7)** and **(4.8)**. After calculating ΔP for each DG, the $P_{generated}$ is updated (adding or subtracting ΔP from the previous value of $P_{generated}$). Then, the new frequency is calculating using equation (3.4). Finally, the algorithm moves back to step 2 to repeat the calculation using the new f_{grid} and $P_{generated}$. In case of the injected power of the slack bus is less than *Tolp* the previous values of f_{grid} and $P_{generated}$ are kept and the algorithm moves to the next step.

Step5: The value of counter c is increased by one.

Step6: If c is greater than the predefined maximum number of iterations, i.e. *MaxIter*, the algorithm terminates, since convergence cannot be achieved. To address this issue, the user should repeat the power flow analysis using a higher value for the integral term k. A detailed analysis for the impact of the integral term on the convergence of the proposed method is presented in step8.

Step7: Reactive power injections of all DG units, i.e., $\boldsymbol{Q}_{dg}$, are computed according to equation **(3.5)**, using $\boldsymbol{V}^{c-1}$.

Step8: Modeling of voltage dependent droop curves using iterative procedures may result in numerical oscillations of the injected powers. These power oscillations result in voltage oscillations. To avoid these spurious oscillations, the approach of adding new nested loop is adopted. More specifically, the power flow is not performed using Q_{dg} injections. On the contrary, for the c-th iteration, the injected reactive powers Q^c are computed considering the values of the previous iteration Q^{c-1}, the values of Q_{dg} as well the value of the integral term k. Q^c is computed as follows:

$$Q^c = Q^{c-1} + \frac{Q_{dg} - Q^{c-1}}{k} \quad (4.11)$$

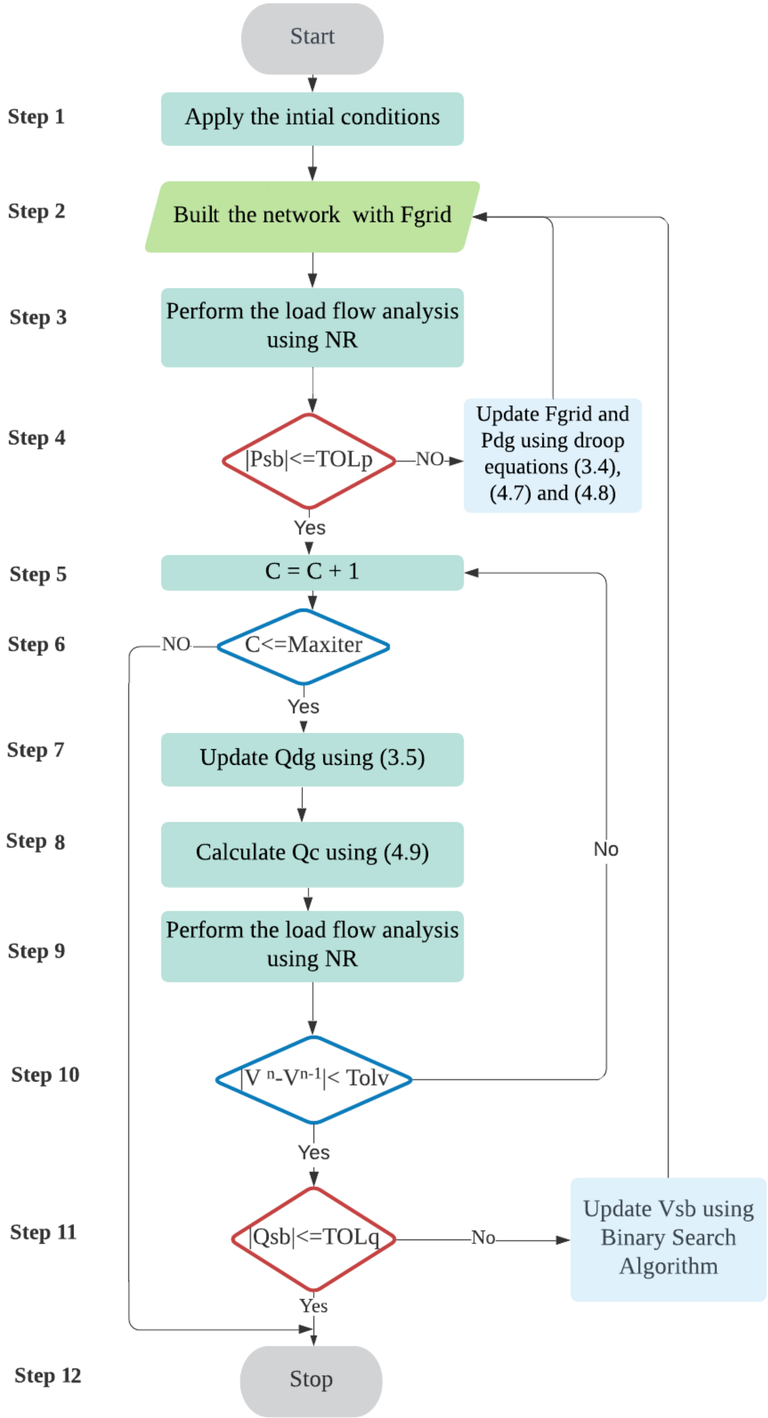

Figure 4.8 flowchart of the second method.

The value of k can vary from small to large values. Small values result in small execution times, but it cannot guarantee the convergence. On the other hand, large values exhibit slow convergence rate, but result in more robust and accurate results. A trade-off between convergence rate and damping of oscillations should be made for the right choice of the integral term. [36]

Step9: Voltages of all MG nodes, i.e., $\boldsymbol{V}^c$, are computed through a power flow analysis using $\boldsymbol{P}_{dg}$, $\boldsymbol{Q}^c$, and f_{grid}. Using the results of this power flow, the reactive power flowing through the slack bus, i.e., Q_{sb}, is calculated.

Step10: A comparison of all node voltages between the last two iterations is performed. If *tolv* criterion is satisfied, the algorithm proceeds to step11; otherwise the algorithm moves back to step 5 and new reactive power injections are computed.

Step11: This step is similar to step 4, where the injected reactive of the slack bus is compared to the reactive power tolerance. In case, where the injected reactive power of slack bus is higher than *Tolq*, the voltage of the slack bus given in step 1 is updated. The new value of the slack bus voltage is calculated using the binary search method (Algorithm 1). After updating the value of the V_{Sb}, the algorithm moves back to step 2 to repeat all the steps. In case, where the injected reactive power of slack bus is less than *Tolq* this means that the calculations are done and the final values of the frequency, the generated active and reactive power, the voltages and phase angles are the desired value for the islanded microgrid load flow solution.

Step12: The procedure terminates providing the power flow solution of the examined MG.

4.2.1.4 Validation of the Second Algorithm

The second algorithm with the added third loop is validated and simulated on the same network presented in **Figure 4.2** in order to see the results in terms of power oscillations and compare it with what we have obtained before. The network was developed in the MATLAB environment using the data demonstrated on the **Table 4.1**.

In equation **(4.11)** when K=1, reactive power Q^c will be the same as Q_{dg} and the algorithm will be similar to that shown in **Figure 4.1**. The results obtained from this proposed algorithm are the same in **Figure 4.3**.

The DGs active and reactive powers are plotted with different values of the integral term K as shown in the following figures:

a) Case 1 :K=1

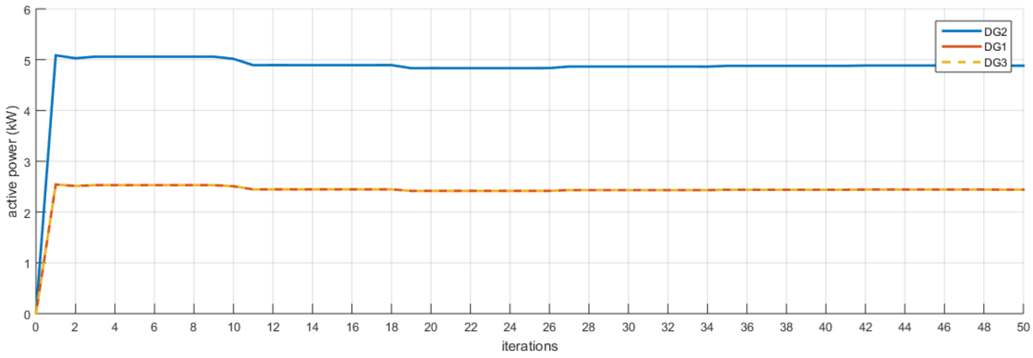

(a)

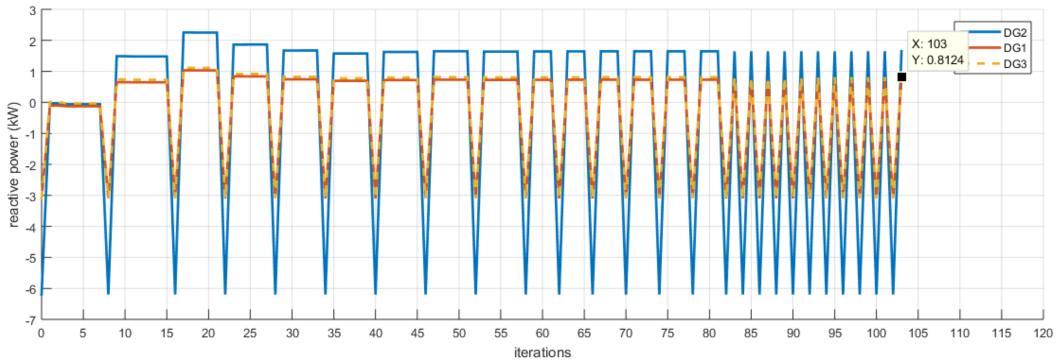

(b)

Figure 4.9 Variation for k=1 of a) active power injection, b) reactive power injection

b) Case 2:K=2

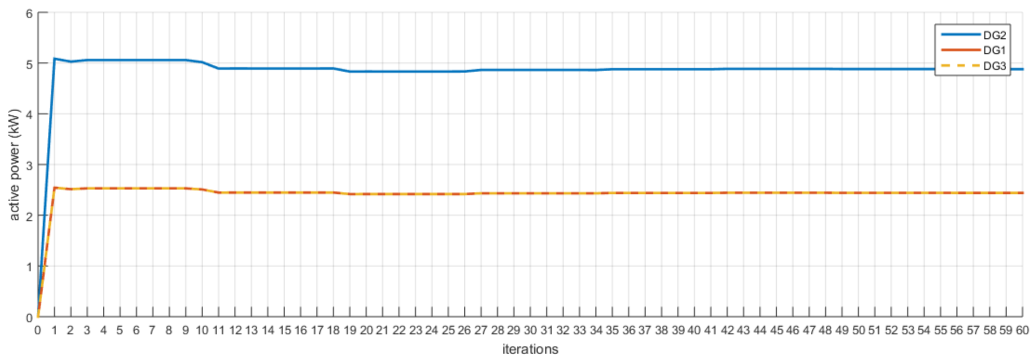

(a)

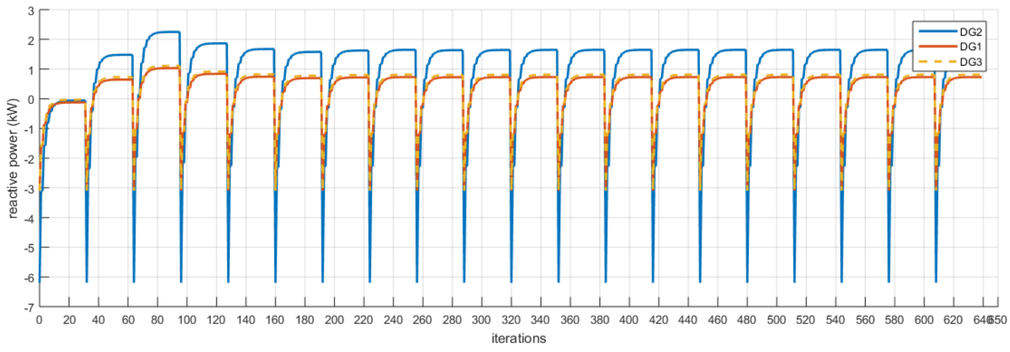

(b)

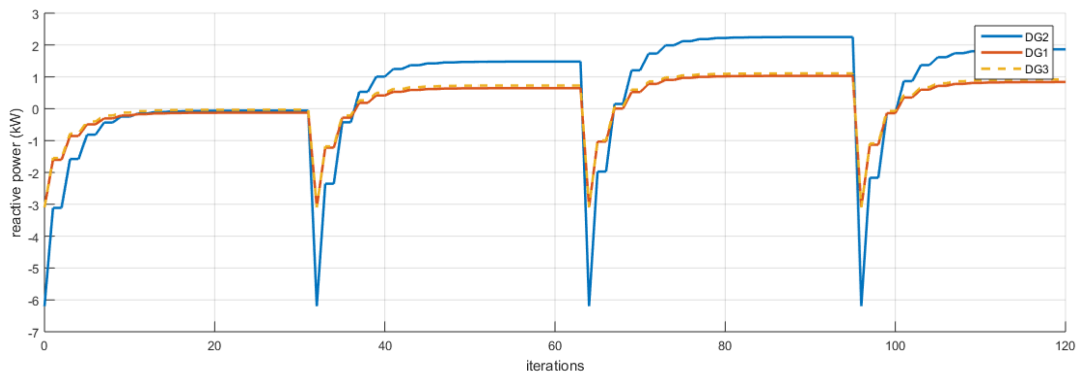

(c)

Figure 4.10 Variation for k=2 of a) active power injection, b) reactive power injection full iterations c) reactive power injection until iteration 120

In order to see more clear results in terms of the change in oscillations, the integral term K is increased to 10.the active and the reactive power that results from the inner loop is plotted as it is shown in the following figures.

c) Case 3:K=10

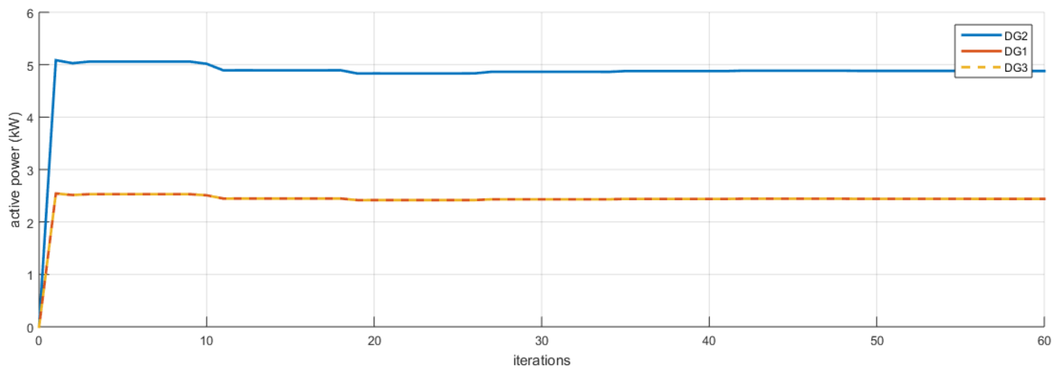

(a)

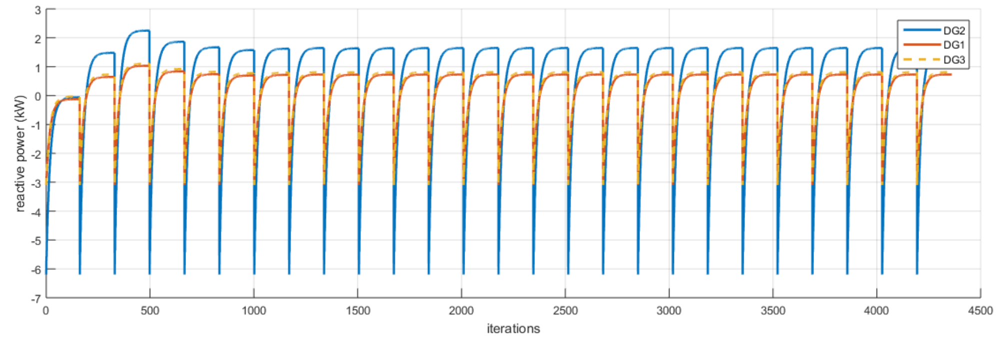

(b)

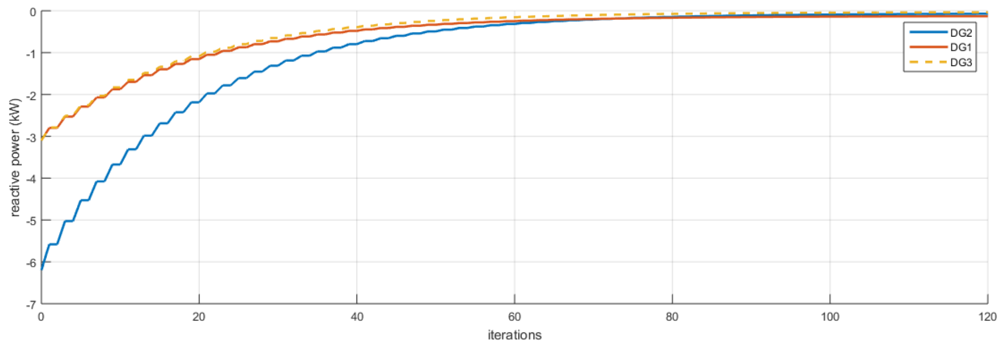

(c)

Figure 4.11 Variation for k=10 of a) active power injection, b) reactive power injection full iterations c) reactive power injection until iteration 120

The execution time of MG simulation is displayed with respect to the change in the integral term K as it is shown in the following figure.

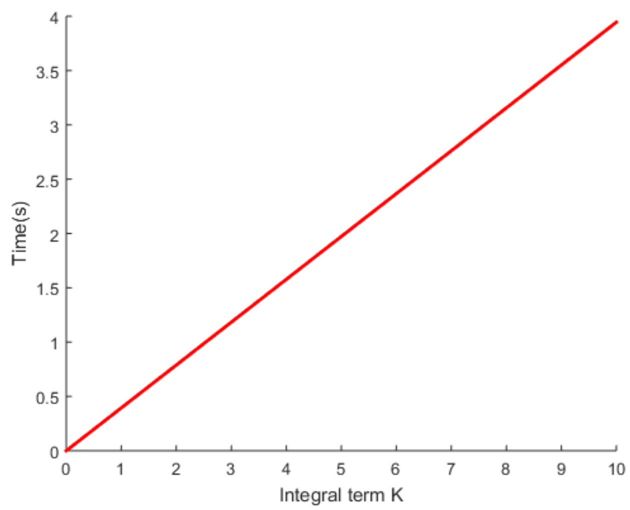

Figure 4.12 Variation of execution time with respect to K

➢ Discussion

a) Case 1 :K=1

- The active power injections start from zero which is the initial value, then it reaches a steady state after a number of iterations.
- The reactive power response shown in **Figure 4.9** reflects the algorithm structure presented before in which three nested loops are validated.
- The graph of the reactive power starts from a negative value that is –Qmax which is the initial value, after that the iterations of the reactive power are performed in the third loop until the condition is satisfied (step 10), then the algorithm perform the outer loop until convergence is reached, starting each time by the same initial conditions –Qmax.
- We could notice that convergence time is extended compared to first algorithm due to the third added loop.

b) Case 2 :K=2

- **Figure 4.10.c** is the zoom picture of **Figure 4.10.b** .We can see from the graph that the active power response does not change as it always starts from the zero which is the initial value, and then it reaches the steady state after a number of iterations, and this is due to the independency from the integral term K such that only the reactive power and voltages will be affected by the increase of this term.
- The reactive power response shown in **Figure 4.10.b** starts by the initial value, then a number of iterations is validated for the first loop then the process performs the added third loop until convergence is satisfied, starting each time by the same initial conditions that is $-Q_{max}$.
- In **Figure 4.9** after performing the first inner loop, the steady state was satisfied in about 10 iterations, however in our case, the response delayed until 20 iterations to reach the steady state, therefore we could notice that convergence time is more extended compared to that in **Figure 4.9** due to the increase of the K value and this is clearly explaining the droop equation **(4.9)** stated before.
- The oscillations in the reactive power observed clearly from the ΔP between iterations so that a remarkable change is deduced. If we take two values of reactive power from two iterations and compare them with the same iterations of the first case (K=1), we will find that Q is increasing slowly.

- One can conclude that bigger k leads to small change in reactive power hence less oscillations and an increase in the convergence time.

c) *Case 3 :K=10*

- **Figure 4.11.c** is the zoom picture of **Figure 4.11.b**. We can see from the graph that the active power response does not change as usual, and this is due to the independency from the integral term K.
- The reactive power response shown in **Figure 4.11.b** starts by the initial value, then a number of iterations is validated for the first loop then the process performs the added third loop until convergence is satisfied, starting each time by negative initial value.
- In the previous case (K=2) after performing the first inner loop, the steady state was satisfied in about 20 iterations, however in our case, the response delayed 80 iterations to reach the steady state, therefore we could notice that convergence time is extended compared to that in previous case due to the increase of the K value.
- The oscillations in the reactive power observed clearly from the ΔP between iterations so that the response get. This can be deduced If we take two values of reactive power from two iterations and compare them with the same iterations of the previous case (K=2), we will find that the mismatch is very small.
- These results confirm for us our conclusion that the bigger the integral factor k the smaller the oscillations of the reactive power, and the longer the convergence time will be.

▪ **Figure 4.12** presents the variations of the execution time with respect to the integral term K. it is clearly observed that the relation between them is linear so that there is a tradeoff between the robustness of the results and the time response, and this clarifies our previous deductions such that as the integral term increases, more time will be needed to satisfy the convergence.

▪ As it is mentioned before; the value of *k* can vary from small to large values. Small values result in small execution times, but cannot guarantee the convergence. On the other hand, large values exhibit slow convergence rate, but result in more robust and accurate results. A trade-off between convergence rate and damping of oscillations should be made for the right choice of the integral term

➢ Conclusion

In all test cases, the method results in very accurate and robust estimates, presenting also low computational burden. The incorporation of the integral term our algorithm intends to reduce oscillations in voltage therefore in the reactive power. However, an increase of the integral term also results in a slower but more robust convergence of the calculation procedure to equilibrium. Therefore, it can be concluded that the proposed algorithm constitutes a reliable tool which can be used for extended low-voltage networks with large DGs contribution.

In order to test the ability of our algorithm shown in **Figure 4.8** to simulate extended electrical networks that comprise DG units, a network of 18 buses is suggested for performing our PFA.

4.2.2. Eighteen Bus Microgrid Simulation

The system under study is presented in **Figure 4.13** and consists of a 0.4 kV islanded MG. This system is based on the topology of the European LV residential distribution grid [38]. The notation and the numbering of nodes in **Figure 4.13** is according to [38]. To derive the LV MG, the following modifications have been applied on the benchmark model of [38]. First, six (6) DG units are connected to nodes R2, R5, R7, R10, R12, and R15. The droop coefficients of all DG units are presented in **Table 4.4**. Additionally, the load connected in node R1 of the benchmark system is intentionally omitted from the LV MG. As discussed in [38], this load represents additional feeders served by dedicated transformers, i.e. this load does not constitute a part of the examined feeder. Thereby it is omitted from the analysis. All other network loads as well as network lines are modeled as discussed in [38].

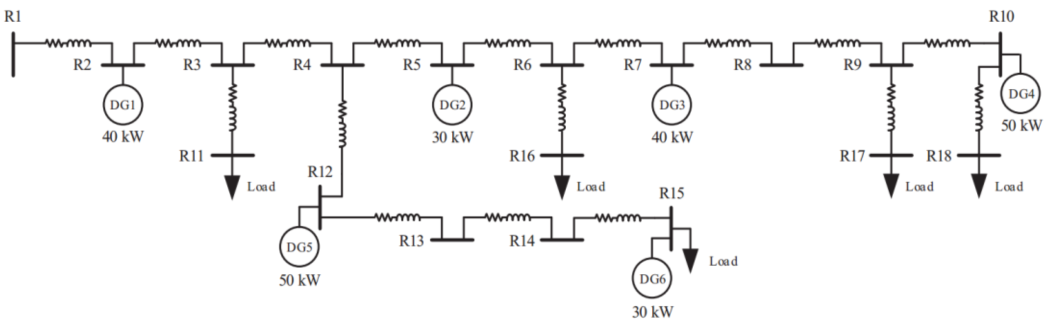

Figure 4.13 Eighteen bus test system.

The initial values used for testing the proposed network are resumed in the following table:

Table 4.4 The initial values of the 18 bus proposed network

Initial Conditions						
Variables	**P_i (KW)**		**Q_i (VAR)**	**V_i**		**δ_i**
Values	Pl(11) = -14.25 Pl(15) = -49.40 Pl(16) = -52.25 Pl(17) = -33.25 Pl(18) = -44.65		Qg(2)=-2.4790 Qg(5) =-1.8592 Qg(7) = -2.4790 Qg(10) =-3.0987 Qg(12) =-3.0987 Qg(15) =-1.8592	440		0
Droop Coefficients						
m_i	**m_1**	**m_2**	**m_3**	**m_4**	**m_5**	**m_6**
Values*(Hz/KW)*	0.05	0.066	0.05	0.04	0.04	0.066
n_i	**n_1**	**n_2**	**n_3**	**n_4**	**n_5**	**n_6**
Value*(V/KVAR)*	1.613	2.151	1.613	1.291	1.291	2.151
Binary Search Algorithm						
Variables	**V_{max}**	**V_{ub}**	**V_{lb}**	**Tol_v**	**Tol_p, Tol_q**	**f (Hz)**
Values	440	440	360	0.0001	0.01	51

4.2.2.1. Validation of the Proposed Network

The proposed algorithm of **Figure 4.8** was developed in the MATLAB environment to solve the power flow problem of our proposed network using the data demonstrated on the table 4.4 however; our developed MATLAB algorithm is not very suitable for extended distribution networks, because of the following characteristics of such systems:

- Radial structure with sometimes weakly-meshed topology.
- High resistance to reactance (X/R) ratio which sometimes causes the NR and the FD methods to diverge
- Untransposed or rarely transposed lines where it is often inappropriate to neglect the mutual coupling between phases.
- Unbalanced loads along with single-phase and double phase laterals.
- Unbalanced distributed loads.
- Dispersed generation. [39]

To solve this problem, a new software tool is presented for the simulation of our networks under steady-state conditions. Its distinct advantage is the robust integration of distributed generation droop controls, while offering the ability to simulate extended networks fast and reliably. The proposed simulation tool is based on the combination of two well-known software products, namely MATLAB and OpenDSS. The latter is employed as an unbalanced power flow solver, whereas the former implements the droop control of DG units. Simulation results for a simple and extended low-voltage network show the effectiveness of the proposed tool and mainly the reduction in the execution times over other conventional time-domain-based software products. [36]

4.2.2.2. OpenDSS Simulation Software

The Open Distribution System Simulator (OpenDSS or simply DSS) is a comprehensive electrical system simulation tool for electric utility distribution systems. OpenDSS is an open source developed by the Electric Power Research Institute [40]. There are two available implementations of OpenDSS, a standalone executable platform and an in-process COM server DLL, which is designed to drive the OpenDSS from a variety of other platforms. The executable version consists of a basic User Interface on the DSS solution engine to help users develop scripts and view solutions. The basic user interface is a text scripting standalone user interface which is sufficient for most of the analysis. The COM interface can be used to design and execute custom solution modes and features of the simulator from any third-party analysis programs like MATLAB, VBA, C#, Python etc. OpenDSS can support all kinds of steady state analysis commonly performed for utility distribution systems. In addition, the most important advantage of OpenDSS is that it supports analysis with distributed generation integration and time series power flow. OpenDSS can be expanded by integrating user developed DLLs to the solution engine to meet future needs.

Some of the important applications of OpenDSS are listed below.

- Distribution Planning and Analysis
- General Multi-phase AC Circuit Analysis
- Analysis of Distributed Generation Interconnections
- Annual Load and Generation Simulations

- Analysis of Unusual Transformer Configurations
- Loss evaluations with unbalanced loadings

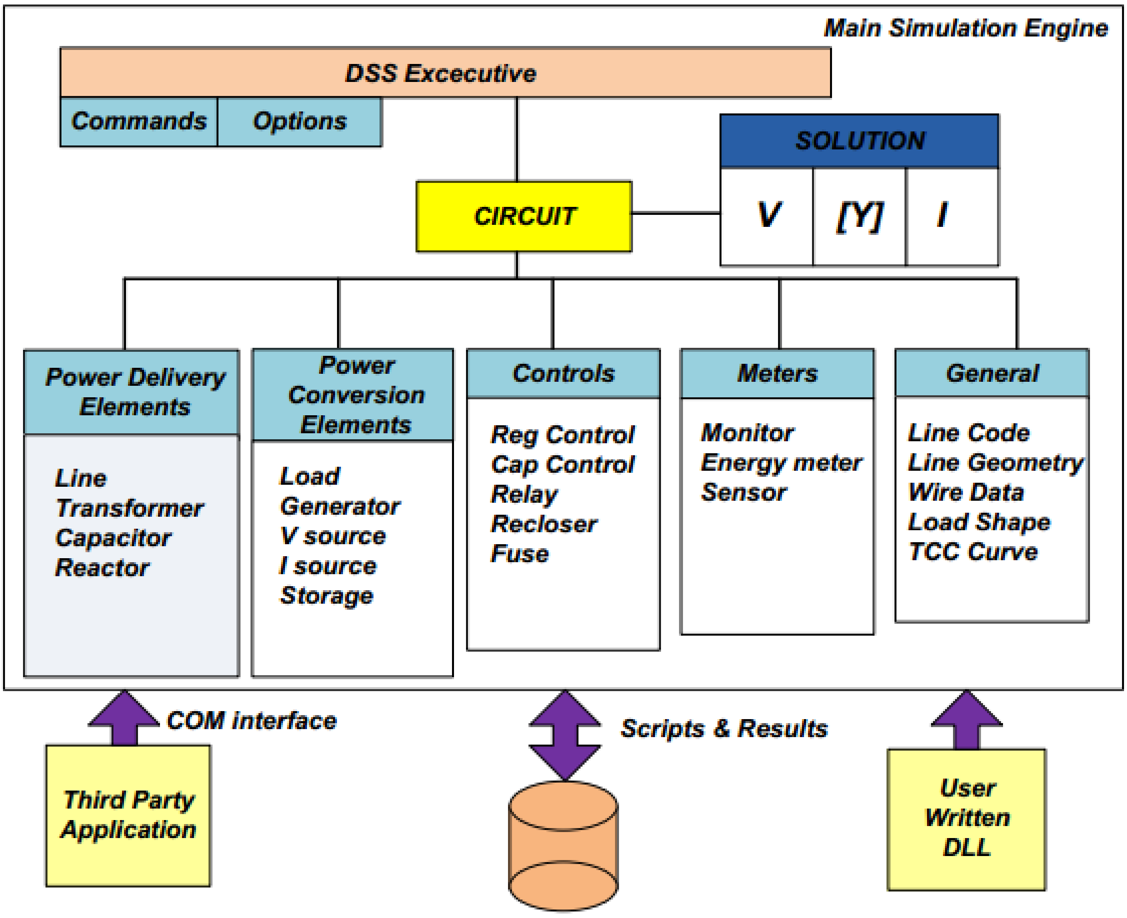

Figure 4.14 OpenDSS architecture

4.2.2.3. Algorithm verification On the Proposed Network

The proposed tool is based on the combination of two software products, namely MATLAB and OpenDSS. The latter is used as an unbalanced power flow solver, employing phase-domain analysis of the network. MATLAB is utilized for the modeling of the developed control schemes and especially the incorporation of droop control for the injected active power of each DG unit.

The voltages, angles, active and reactive power are shown in the following figure:

```
Command Window
*********************** Results ********************************
-----------Voltages (V) ---------  Angles (degrees)------------
bus_1       384.7499               0.0000
bus_2       384.7499               0.0000
bus_3       384.1992               -0.0152
bus_4       383.8942               -0.0250
bus_5       383.3259               -0.0413
bus_6       382.3383               -0.0677
bus_7       382.2614               -0.0737
bus_8       381.6189               -0.0916
bus_9       380.9764               -0.1095
bus_10      380.9136               -0.1145
bus_11      383.2516               0.0158
bus_12      385.0862               -0.0608
bus_13      383.1439               -0.0140
bus_14      381.2018               0.0333
bus_15      379.5374               0.0742
bus_16      378.8225               0.0480
bus_17      378.7387               -0.0356
bus_18      377.9020               -0.0150
****************************************************************
------- Real Powers P(KW)-------- Reactive Powers Q(KVAR)----
DG_1       32.6250                    9.4511
DG_2       24.4688                    7.7502
DG_3       32.6250                    10.9933
DG_4       40.7813                    14.7858
DG_5       40.7813                    11.5534
DG_6       24.4688                    9.5112
**************************************************************
--Frequency(Hz) --Excution time(s)--Iteration-----------------
     49.3687              23.5742            20
fx **************************************************************
```

Figure 4.15 Eighteen bus network simulation results

The time domain simulation has been performed using PSIM software in [3], then the active and reactive power of the DGs are displayed in the **Table 4.5**.

Table 4.5 Active (KW), and reactive (KVAR)power of the DG units using PSIM

Active (KW) and Reactive (KVAR) Powers						
DG_i	**1**	**2**	**3**	**4**	**5**	**6**
P_{Psim}	32.625001	24.468759	32.625001	40.781265	40.781265	24.468759
$P_{Proposed}$	32.6250	24.4688	32.6250	40.7813	40.7813	24.4688
Q_{Psim}	9.451056	7.750209	10.993335	14.785813	11.55335	9.511234
$Q_{Proposed}$	9.4511	7.7502	10.9933	14.7858	11.5534	9.5112

- **Comparison**

- TD simulations in [3] are performed using PSIM software. All their simulations are performed using an Intel Core i7-930, 2.8 GHz, RAM 24 GB, personal computer.
- Our algorithm is validated using Intel Core i3-311M, 2.4 GHz, RAM 4 GB, personal computer.
- The errors in terms of active power and reactive power are negligible as well as the voltages.
- In [3] to simulate the first three seconds and to reach the steady-state condition, PSIM requires approximately 2958 s. The MG frequency in the new steady-state is equal to49.36869 Hz.
- The simulation time of our algorithm using MATLAB interfaced with DSS is 23.5742s, whereas the execution time in [3] takes 11.3s. This difference in time is actually due to the type of computer that we used that it not comparable with their computer.
- The execution time could be reduced with good performance computer.
- The initial conditions changes don't really affect the results too much.
- It could be noticed that the openDSS interfaced with MATLAB softwares are valuable tools for performing the power flow and getting better results. One drawback that could be faced is the considerable execution time which is related to the type of computer.

For different integral terms Ks the active and reactive powers are displayed and compared each time as follow in the figures below.

a) Case 1:K=1

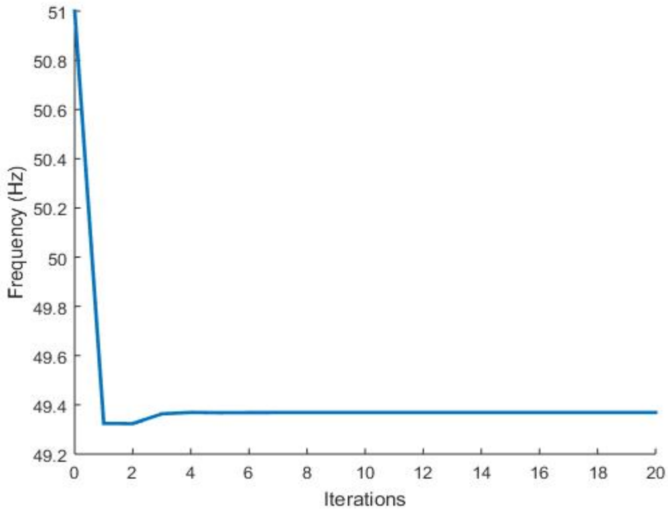

(a)

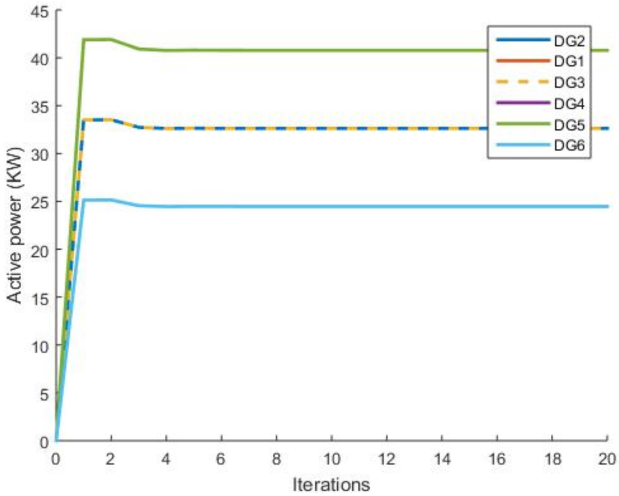

(b)

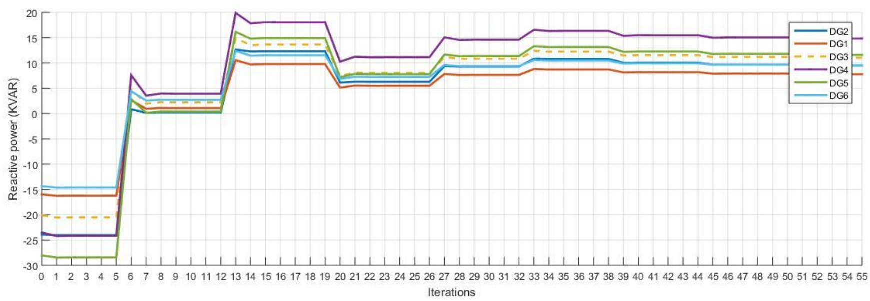

(c)

Figure 4.16 First case resultant a) frequency, b) active power, c) reactive power

b) Case 2:K=2

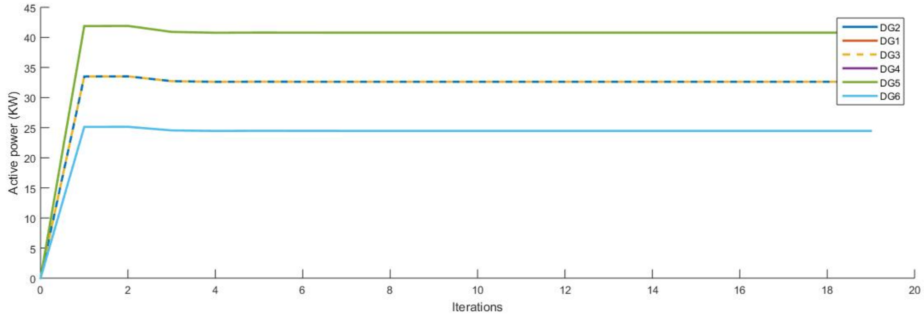

(a)

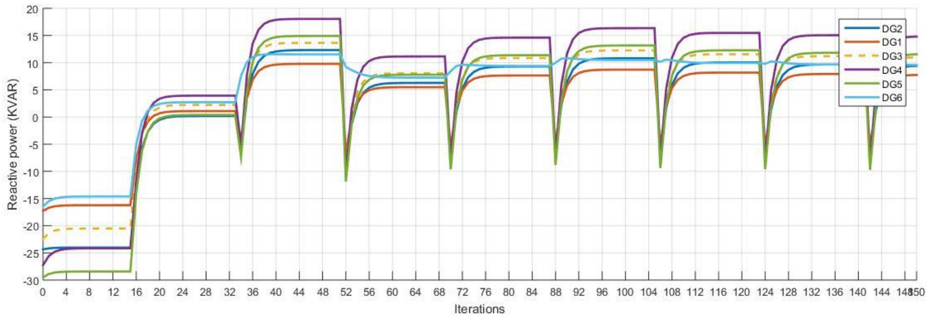

(b)

Figure4.17 Second case resultant a) active power, b) reactive power

c) Case 3:K=10

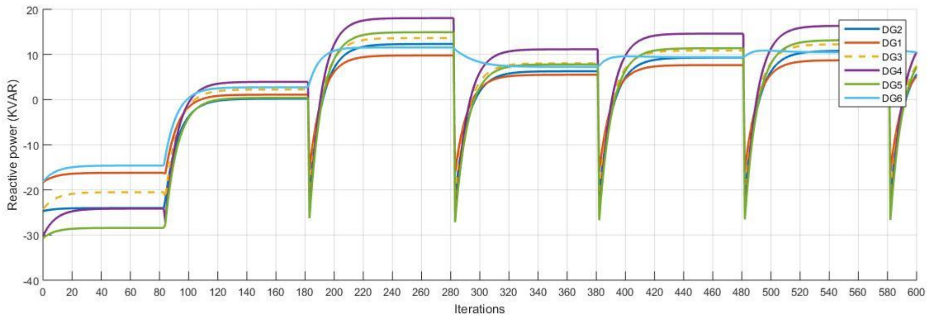

Figure 4.18 Last case resultant reactive power

The execution time of MG simulation is displayed with respect to the change in the integral term K as it is shown in the following figure.

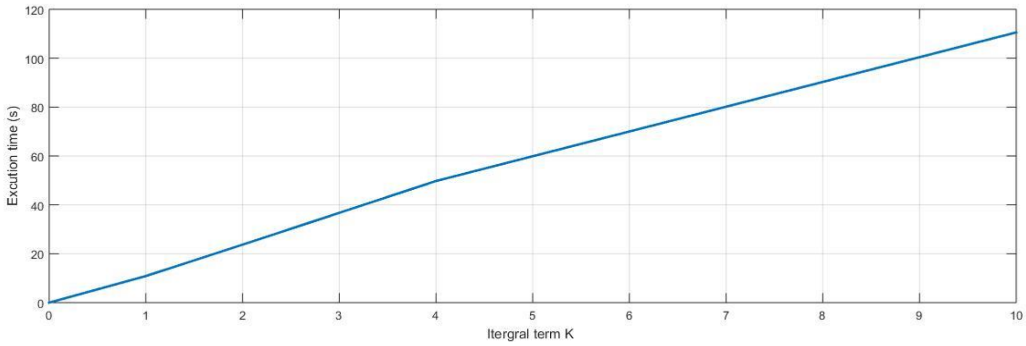

Figure 4.19 Variation of execution time with respect to K

Discussion

a) Case 1 :K=1

- For the first graph (**Figure 4.16.a**) we could notice that the frequency of the network starts from 51Hz which is the initial value stated on the algorithm, along with the iterations the frequency decreases gradually as the DGs active power increases, and this satisfies the equation **(3.4)**.The frequency stabilize finally at 49.3687Hz after some number of iterations as it is checked in **Figure 4.15**.
- For the first case we can see that the active power starts from the zero which is the initial value, and then it reaches the steady state after a small number of iterations.
- The reactive power response shown in **Figure 4.16.c** reflects the algorithm structure presented before in which three nested loops are validated .The graph starts from a negative value that is $-Q_{max}$ which is the initial value, after that the iterations of the reactive power are performed in the inner loop until the condition is satisfied (step 11), then the algorithm perform the outer loop until convergence is reached, starting each time by the same initial conditions $-Q_{max}$.

b) Case 2 :K=2

- For the second case we can see from the graph that the active power response is the same as in the previous case, and this is due to the independence from the integral term K such that only the reactive power and voltages will be affected by the increase of this term.
- The reactive power response shown in **Figure 4.17.b** starts by the initial value, then a number of iterations is validated for the first loop then the process performs the

outer loop until convergence is satisfied, starting each time by the same initial conditions that is $-Q_{max}$.

- In our case, the response takes more time to stabilize compared to the case 1, therefore we could notice that convergence time is increased due to the increase of the K value.
- The oscillations in the reactive power observed clearly from the ΔP between iterations so that a remarkable change is deduced. If we take two values of reactive power from two iterations and compare them with the same iterations of the first case (K=1), we will find that Q is increasing gradually taking more iterations.
- One can conclude that bigger k leads to small change in reactive power hence less oscillations and an increase in the convergence time.

c) Case 3 :K=10

- For the last case we can see from the graph that the active power response does not change as usual.
- The reactive power response shown is in **Figure 4.18** the convergence time is increased compared to that in previous case due to the increase of the K value.
- The oscillations in the reactive power observed clearly from the ΔPso that they are reduced and the algorithm gives more robustness on our network.
- **Figure 4.19** presents the variations of the execution time with respect to the integral term K. it is clearly observed that the relation between them is almost linear, and this clarifies our previous deductions such that as the integral term increases, more time will be needed to satisfy the convergence.

Conclusion

The performance of the proposed algorithm is further demonstrated in an extended 18-node network with loads. Results show that the execution time is slightly affected by the size of the network, making the proposed software a powerful tool for the efficient simulation of extended distribution grids with controlled DG units.

4.2.3. Six Bus Microgrid Simulation

To validate our proposed algorithm, a 6-bus system is chosen with rated voltage of 127, as shown in **Figure 4.20**. This system operates in an islanded mode and consists of three droop control DGs, setting on buses 4, 5 and 6. The load and line data of the system are based on [41].

In this network, all these three generator buses are taken as dispatchable buses; all the lines are with resistance to inductance ratio R/X approximately as 7.7 to mimic the typical low voltage lines. the parameters of the circuit are presented in **Table 4.6**. [42]

Table 4.6 Control parameters of DG units in six-bus system [42]

Parameters	Symbols	Values	Units
Line resistance	**R (i,j)**	0.15	**Ω**
Line inductance	**L (i,j)**	0.062	**mH**
LC filter inductor	**L_{DG} (i)**	1.8	**mH**
LC filter capacitance	**L_{DG} (i)**	27	**μF**
Load Parameters			
Bus number	**R_{Load}(Ω)**		**L_{Load}(H)**
Bus 4	90		0.0609
Bus 5	110		0.0836
Bus 6	100		0.25136
Control Parameters			
Parameters	**DG_1**	**DG_2**	**DG_3**
Proportional frequency (m) $[\frac{rad}{W*S}]$	0.001	0.005	0.004
Proportional amplitude (n)$[\frac{V}{VAR}]$	0.02	0.01	0.02
Virtual Resistor (Ω)	0.1	0.1	0.1
Virtual Inductor (H)	0.004	0.004	0.004

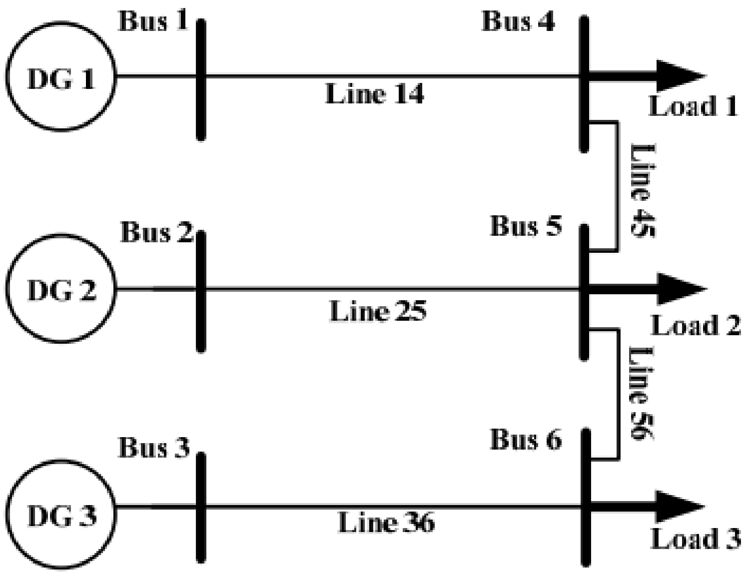

Figure 4.20 Six bus test system

4.2.3.1 Validation of Six-bus Network

The first algorithm is validated and simulated on the network presented in **Figure 4.20** in order to see the results. The network was developed in the MATLAB software interfaced with openDSS environment. The voltages, angles, active and reactive power are shown in the **Figure 4.21**.

To show the improvement of the proposed power flow analysis, power flow results from the proposed method are compared with those from several conventional methods by reference to the steady state of time domain simulation using SimPowerSystem used in [42]. The results are presented on the table 4.7.

It can be seen that the relative error of magnitude deviation compared with simulation is about 8%. The good agreement between the results indicates the accuracy of the proposed power flow analysis in solving the LV microgrid networks with droop controller and virtual impedance.

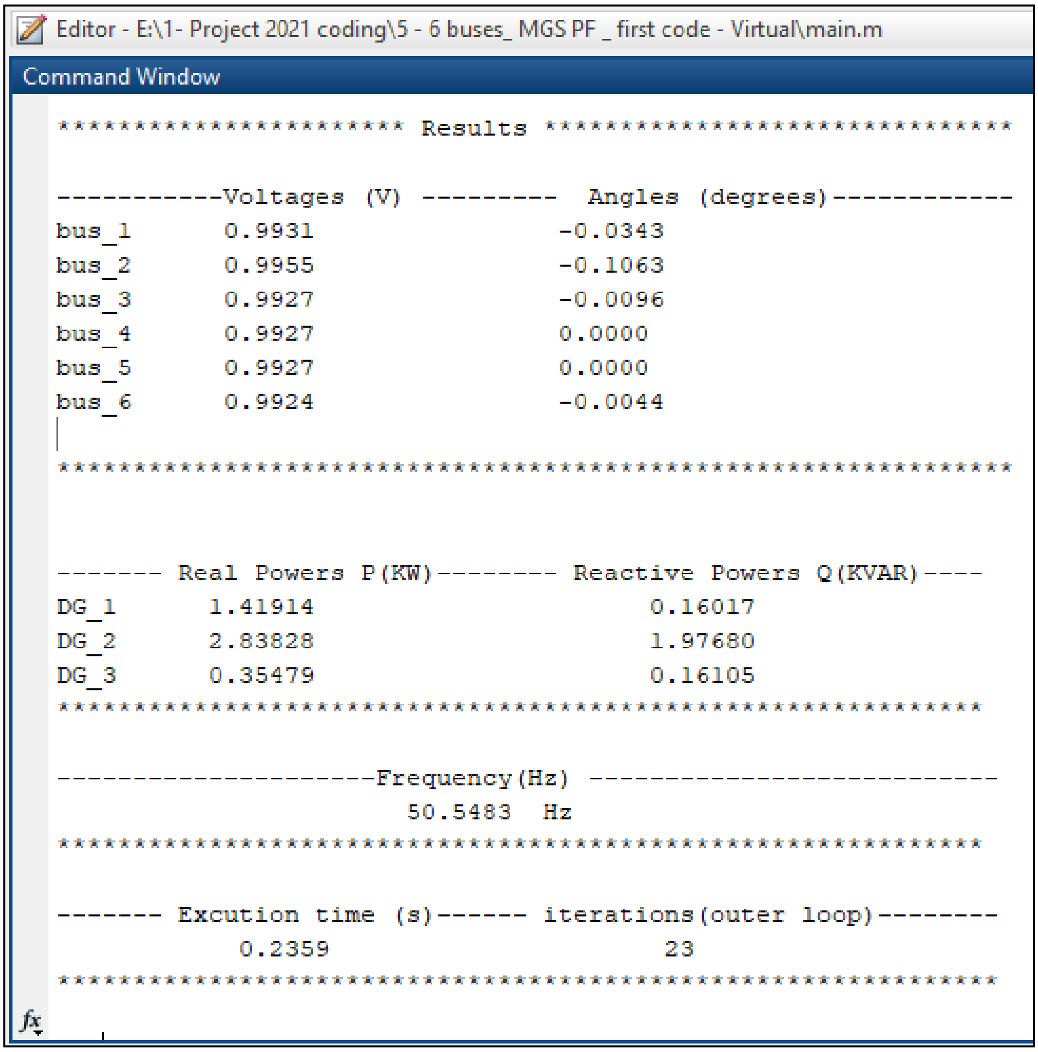

Figure 4.21 Six bus system results

Table 4.7 Validation results of the six bus AC microgrid [42]

Bus number	Simulator results		Power Flow results		Percent Error (%)
	Voltage (V)	Angle (degree)	Voltage (V)	Angle (degree)	
1	0.9629	0.000	0.9931	0.03	3.13
2	0.9645	0.015	0.9955	0.016	3.21
3	0.9624	0.052	0.9927	0.009	3.14
4	0.9618	0.004	0.9927	0.00	3.21
5	0.9623	0.020	0.9927	0.00	3.15
6	0.9619	0.053	0.9924	0.044	3.17

4.3. Conclusion

In this chapter, two algorithms are proposed to solve the load flow of islanded MG problem. The first methodology is proposed to accurately solve the power flow problem in AC MGs. The distinct advantage of the method is its computational efficiency compared to the time-consuming TD simulations. A three-nested-loop iterative procedure is developed to extend the applicability of CPF methods for the analysis of islanded MGs. These algorithms are tested on three different MG networks the outputs results are compared with the time domain solution. In all test cases, the second proposed method results in very accurate and robust estimates. Therefore, it can be concluded that the proposed method constitutes a valuable tool which can be used for the power flow analysis of islanded MGs.

General Conclusion

When microgrids get isolated from the main grid, it displays unique behaviors that can present challenges during the design process, specifically power flow studies. Islanded microgrids characteristics include the absence of an infinite bus that keeps the frequency and voltage constant. Therefore, a new approach is needed to calculate the power flow of (networked) AC MGs.

This research has presented power flow analysis tools that endeavor to address the challenges mentioned above. In particular, the main contributions of this thesis are summarized below.

Two load flow solutions with the droop control characteristics are presented for the islanded microgrid. The first solution was based on the Newton-Raphson algorithm, which is the most used deterministic and conventional load flow technique that depends on the initial guesses. The distinct advantage of the method is its computational efficiency compared to the time-consuming TD simulations. Towards the objective of having efficient results with less oscillation in reactive power, a three-nested-loop iterative procedure is developed to extend the applicability of CPF methods for the analysis of islanded MGs. These algorithms are tested on a 7-bus, 18-bus and 6-bus micro-grids. OpenDSS software is used with MATLAB to simulate the networks and the outputs results are compared with the time domain solution outcomes using specified software PSIM that validate the accuracy of the proposed techniques. In all test cases, the method results in very accurate and robust estimates, presenting also close values to time simulation. The Objective is achieved and the proposed algorithms provide a satisfactory performance, especially for the extended network with more DGs contribution. Therefore, it can be concluded that the proposed method constitutes a reliable tool which can be used for the power flow analysis of islanded MGs

Building upon the power flow analysis methods developed in this research; there are several avenues for future works in the planning of networked islanded microgrids which are:

- Performance of the proposed networks using meta-heuristic algorithm.
- Performing DC load flow analysis and compare it with AC PFA in each network
- Testing our algorithm on bigger networks with different simulation softwares.

References

[1] Baochao WANG, Doctorate theses ,‘’Intelligent control and power flow optimization of microgrid. Energy management strategies’’ Laboratoire AVENUES-GSU, EA 7284,December 2012.

[2] Ernauli Christine Aprilia, Doctorate theses , ‘’Power Flow Analysis tool for networked islanded hybrid AC/DC’’ Laboratoire School of Electrical Engineering and Telecommunications Faculty of Engineering, February 2012.

[3] Elefherios O. Kontis, Georgios C. Kryonidis, Angelos I. Nousdilis, Kyriaki-Nefeli D. Malamaki, and Grigoris K. Papagiannis, “Power flow of islanded ac microgrids,” *IEEE Trans.* July 2019

[4] [online]: https://lo3energy.com/find-energy-industry-needs-microgrids-work-now-work-future/ February 16, 2018

[5] https://www.tdworld.com/digital-innovations/article/20970388/a-short-history-the-microgridOCT 24, 2017

[6] Patel N., Porwal D., Bhoi A.K., Kothari D.P., Kalam A ,‘’An Overview on Structural Advancements in Conventional Power System with Renewable Energy Integration and Role of Smart Grids in Future Power Corridors”. https://doi.org/10.1007/978-981-15-4246-6_12020

[7] M.Paul, J.Miller, S.Knudsen, T.Grabowski. “Electric Power System Asset Optimization”. 2011.

[8] T.T. SON, Doctorate theses, “Islanding detection and power quality analysis in’’, Shibaura Institute Of TechnologySeptember 2019.

[9] M.S. Mahmoud, ‘’ Microgrid Control Problems and Related Issues’’, www.studentenergy.org ,2017.

[10] [online]: https://microgridknowledge.com/energy-storage-microgrid/

[11] R. Arghandeh; M. Pipattanasomporn; S. Rahman,‘’Flywheel Energy Storage Systems for Ride-through Applications in a Facility Microgrid ’’,*IEEE Trans.*04 September 2012

[12] Yogita Pradhan, Shweta Mishra , M. ‘’Review On Development Of Microgrid With Renewable Energy Sources‘’, ITM university, Raipur (Chhattisgarh), India 2019

[13] Xi-Fan Wang, Yonghua Song, Malcolm Irving, ‘’Modern Power Systems Analysis‘’. 1sted,2008

[14] [online]: https://presentgroup.com.au/types-of-buses-in-a-load-flow-analysis/

[15] [online]: https://circuitglobe.com/bus-admittance-matrix.html

[16] P.S.R Murty, Power System Analysis.1st ed, 2007

[17] A.A. Maske1,"Determination of Power Flow In PQ Bus System By Using Gauss Seidel Method", American Journal of Engineering Research (AJER), vol. 6, no. 12, 2017, pp. 267 271.

[18] J. Duncan Glover, Mulukutla S. Sarma, Thomas Overbye, Power System Analysis and Design Method. 5th ed, Cengage Learning ,2011

[19] [online] :https://top10electrical.blogspot.com/2015/09/limitations-of-gauss-seidel-method-for.html September 19, 2015

[20] C. K. Seng1, T. L. Tien , J. Nanda, Syafrudin Masri1 , "Load Flow Analysis Using Improved Newton-Raphson Method ", 1School of Electrical and Electronic Engineering, UniversitiSains Malaysia; Engineering Campus.

[21] J. Duncan Glover, Mulukutla S. Sarma , Thomas Overbye , power system Analysis and Design .5th ed

[22] van Amerongen, R.A.M, "A general-purpose version of the fast decoupled load flow",IEEE Transactions on Power Systems; volume 4, issue 2 (1989)

[23] Achitavijarvargia, sweetyjain, sehaamena," Methodologies by Analyzing Various Bus Systems", International Journal of Electrical Engineering. Volume 9, Number 2 (2016), pp. 127-138

[24] Ochi, T.; Yamashita, D.; Koyanagi, K.; Yokoyama, R, "The development and the application of fast decoupled load flow method for distribution systems with high R/X ratios lines", IEEE trans ,2013

[25] [online]: https://www.allumiax.com/blog/power-flow-analysis

[26] RohaizahbtMohd Ghazali1, Mathan a , "Power Flow Analysis considering newton raphson, Gass Seidel and Fast Decoupled Mthods ", Department of Engineering, Faculty of Engineering and Life Sciences, Universiti Selangor, Malaysia

[27] Jiao-Jiao Deng1 and Hsiao-Dong Chiang , "Convergence Region of Newton Iterative Power Flow Method:Numerical Studies," School of Electrical Engineering and Automation, Tianjin University.

[28] Mohammed E. Nassar ,1, M.M.A. Salama; S. Rahman‘’ A novel branch-based power flow algorithm for islanded AC microgrids’’,*IEEE Trans.* 11 January 2017

[29] MONICA P , doctorate theses “Droop Control of Parallel Operated Power Converters for Accurate Current Sharing in Islanded AC and DC Microgrids, “ June 2020 [31]

[30] NaserMahdaviTabatabaei, ErsanKabalci, NicuBizon ‘’ Microgrid Architectures, Control and Protection Methods’’ pp 527-554, 1st ed. 2020

[31] Chandorkar M, Divan D, Adapa R. Control of parallel connected inverters in standalone ac supply systems. IEEE Transactions on Industry Application 1993;29(1):136–43(this reference could be of[18]chapter 3)

[32] A.Bidram, A.Davoudi, "Hierarchical Structure of Microgrids Control System," Smart Grid, IEEE Transactions on , vol.3, no.4, pp.1963,1976, Dec.2012.

[33] G. C. Kryonidis, E. O. Kontis, A. I. Chrysochos, K. O. Oureilidis, C. S .Demoulias, and G. K. Papagiannis, “Power flow of islanded ac microgrids: Revisited,” IEEE Trans. Smart Grid, vol. 9, no. 4, pp. 3903– 3905, July 2018

[34] F. Mumtaz, M. H. Syed, M. A. Hosani, and H. H. Zeineldin, “A novel approach to solve power flow for islanded microgrids using modified newton raphson with droop control of dg,” *IEEE Trans. Sustai. Energy*, vol. 7, no. 2, pp. 493–503, Apr. 2016

[35] BELAHADJI Chaima, ZAOUI Hadjer, “Load Flow Solution of Islanded Microgrids Using Conventional and Non Conventional Methods,” July 2019.

[36] G. C. Kryonidis, E. O. Kontis, A. I. Chrysochos, C. S. Demoulias, D. Bozalakov, B. Meersman, T. L. Vandoorn, and L. Vandevelde, “A simulation tool for extended distribution grids with controlled distributed generation,” in 2015 IEEE Eindhoven PowerTech, June 2015.

[37] D. Fetzer, G. Lammert, S. Gehler, J. Hegemann, R. Schmoll, and M. Braun, “Integration of voltage dependent power injections of distributed generators into the power flow by using a damped newton method,” *Int. J. Electr. Power Energy Syst.*, vol. 99, pp. 695–705, 2018

[38] *Benchmark Systems for Network Integration of Renewable and Distributed Energy Resources*. Cigre Task Force C6.04, Technical Report,2014.

[39] S. Elsaiah,M. Ben-Idris,J. Mitra, “Power Flow Analysis of Radial and Weakly Meshed Distribution Networks,” *IEEE Trans. Sustai. Energy*, vol. 7, no. 2, pp. 493–503, Apr. 2016.

[40] *Open DSS Manual*, Electric Power Research Institute, July 2010

[41] Mohammad H. Moradi, VahidBahramiForoutan, Mohammad Abedini, “Power flow analysis in islanded Micro-Grids via modeling different operational modes of DGs: A review and a new approach,” *IEEE Eindhoven PowerTech* 12 November 2016

[42] Li, C., Chaudhary, S. K., Savaghebi, M., Quintero, J. C. V., & Guerrero, J. M. (2017). “Power Flow Analysis for Low-Voltage AC and DC Microgrids Considering Droop Control and Virtual Impedance”. IEEE Transactions on Smart Grid, 8(6), 2754 - 2764 . https://doi.org/10.1109/TSG.2016.2537402